Supplement of Biogeosciences, 23, 21–38, 2026
https://doi.org/10.5194/bg-23-21-2026-supplement

Supplement of

Archaeal lipostratigraphy of the Scotian Slope shallow sediments, Atlantic Canada

Narges Ahangarian et al.

Correspondence to: Narges Ahangarian (narges.ah@hotmail.com) and G. Todd Ventura (todd.ventura@smu.ca)

Table of Contents

S1. Supplemental Text

S1.1 Chemotaxonomic relationships

In marine environments, isoprenoidal GDGTs are the main lipids synthesized by ammonia-oxidizing Thaumarchaeota that inhabit both the surface ocean and mesopelagic zone (Sinninghe Damsté et al., 2002; Schouten et al., 2002; Church et al., 2010; Villanueva et al., 2015; Zeng et al., 2019). However, members of Phylum Thaumarchaeota have different compositions of IPL and CL-GDGTs, depending on their habitat (Bale et al., 2019; Elling et al., 2017). IPLs, in addition to taxonomy, could be reflective of various habitats of Thaumarchaeota (Elling et al., 2017).

With respect to individual IPL classes, 1G-GDGTs, 2G-GDGTs, and 2G-OH-GDGTs are abundant in all Thaumarchaeotal strains (Elling et al., 2017, 2015) and have been used for tracing planktonic thaumarchaeal biomass (Elling et al., 2017) in the marine water column (Schubotz et al., 2009; Schouten et al., 2012; Wakeham et al., 2012; Basse et al., 2014; Xie et al., 2014). Additionally, the synthesis of 1G-GDGTs and GDGTs at seep sediments is also attributed to Bathyarchaeia, previously known as the miscellaneous Crenarchaeotal group (MCG) (Zhang et al., 2023) and may be a reflection of the elevated lipid abundances that are found in these settings.

For CLs, OH-GDGTs have been widely detected in marine environments (Liu et al., 2012b; Huguet et al., 2013; Varma et al., 2024a; Elling et al., 2017; Sinninghe Damsté et al., 2012; Liu et al., 2012b). They are absent in Thaumarchaeota group I.1b, but abundant in Thaumarchaeota group I.1a (Schouten et al., 2013). Unspecified Crenarchaeota or Euryarchaeota have been proposed to synthesize OH-GDGTs (Lü et al., 2015). High temperature enhances production of OH-GDGTs with a higher degree of cyclization (Lü et al., 2015; Umoh et al., 2022). Culture experiments indicated organisms have different compositions of GDGTs and OH-GDGTs (Elling et al., 2017; Bale et al., 2019) and IPL OH-GDGTs in their membrane (Elling et al., 2015, 2017), which can be used as taxonomic indicator within strains of phylum Thaumarchaeota. Cren′ has been detected in living archaeal cells such as ‘‘*Ca.* Nitrosotenuis *uzonensis*” indicating it is not a product of diagenesis (Sinninghe Damsté et al., 2018). Higher production could indicate biological adaptation to environmental stresses, such as high temperature, as the membrane of some thermophilic Thaumarchaeota contain high abundances of Cren′ (Pitcher et al., 2010; Sinninghe Damsté et al., 2012). Low contents of GDGT-1 to -3 and Cren′ with relatively high concentration of Cren and GDGT-0 in environmental samples indicate non-thermophilic Thaumarchaeota source of GDGTs (Schouten et al., 2000; Schouten et al., 2013; Schouten et al., 2002). GDGT-0 is also produced by methanogenic Euryarchaeota (Blaga et al., 2009). Archaeol is synthesized by members of Euryarchaeota, Crenarchaeota, and

Thaumarchaeota (Koga et al., 1993). In environmental samples, the detection of AR is mainly associated with methanogens (Pancost et al., 2011) and ANME (Rossel et al., 2008).With regards to CL-DPs, putative GDDs are widely detected in marine sediments (Knappy and Keely, 2012) where they are regarded as either membrane components or intermediate structures in GDGT biosynthesis (Meador et al., 2014; Coffinet et al., 2015; de Bar et al., 2019) or degradation products of GDGTs (Lui et al., 2012; Coffinet et al., 2015; Mitrović et al., 2023; Hingley et al., 2024). IPL-based GDDs have been detected in cultures of various methanogenic archaea, such as *Methanosarcina mazei* and *Methanosphaera stadtmanae* (Liu et al., 2012; Meador et al., 2014; Bauersachs et al., 2015), implying that GDDs are also biosynthesized by living organisms although the exact pathways have not been determined. 1G-GDDs were reported in Ca. *N. maritimus* (Elling et al., 2014; Meador et al., 2014b), and high abundances of both GDDs and 1G-GDDs are reported in *N. viennensis* strains of phylum Thaumarchaeota (Elling et al., 2017).

S.1.2 References

Bale, N. J., Palatinszky, M., Rijpstra, W. I. C., Herbold, C. W., Wagner, M., and Sinninghe Damsté, J. S.: Membrane Lipid Composition of the Moderately Thermophilic Ammonia-Oxidizing Archaeon "*Candidatus* Nitrosotenuis uzonensis" at Different Growth Temperatures, Appl. Environ. Microbiol., 85, e01332-19, https://doi.org/10.1128/AEM.01332-19, 2019.

de Bar, M. W., Rampen, S. W., Hopmans, E. C., Sinninghe Damsté, J. S., and Schouten, S.: Glycerol ether lipids in sediment core Bass River Site, https://doi.org/10.1594/PANGAEA.897918, 2019.

Basse, A., Zhu, C., Versteegh, G. J. M., Fischer, G., Hinrichs, K.-U., and Mollenhauer, G.: Distribution of intact and core tetraether lipids in water column profiles of suspended particulate matter off Cape Blanc, NW Africa, Org. Geochem., 72, 1–13, https://doi.org/10.1016/j.orggeochem.2014.04.007, 2014.

Bauersachs, T., Weidenbach, K., Schmitz, R. A., and Schwark, L.: Distribution of glycerol ether lipids in halophilic, methanogenic and hyperthermophilic archaea, Org. Geochem., 83–84, 101–108, https://doi.org/10.1016/j.orggeochem.2015.03.009, 2015.

Blaga, C. I., Reichart, G.-J., Heiri, O., and Sinninghe Damsté, J. S.: Tetraether membrane lipid distributions in water-column particulate matter and sediments: a study of 47 European lakes along a north–south transect, J. Paleolimnol., 41, 523–540, https://doi.org/10.1007/s10933-008-9242-2, 2009.

Church, M. J., Wai, B., Karl, D. M., and DeLong, E. F.: Abundances of crenarchaeal *amoA* genes and transcripts in the Pacific Ocean, Environ. Microbiol., 12, 679–688, https://doi.org/10.1111/j.1462-2920.2009.02108.x, 2010.

Coffinet, S., Huguet, A., Williamson, D., Bergonzini, L., Anquetil, C., Majule, A., and Derenne, S.: Occurrence and distribution of glycerol dialkanol diethers and glycerol dialkyl glycerol tetraethers in a peat core from SW Tanzania, Org. Geochem., 83–84, 170–177, https://doi.org/10.1016/j.orggeochem.2015.03.013, 2015.

Elling, F. J., Könneke, M., Lipp, J. S., Becker, K. W., Gagen, E. J., and Hinrichs, K.-U.: Effects of growth phase on the membrane lipid composition of the thaumarchaeon Nitrosopumilus maritimus and their implications for archaeal lipid distributions in the marine environment, Geochim. Cosmochim. Acta, 141, 579–597, https://doi.org/10.1016/j.gca.2014.07.005, 2014.

Elling, F. J., Könneke, M., Mußmann, M., Greve, A., and Hinrichs, K.-U.: Influence of temperature, pH, and salinity on membrane lipid composition and TEX86 of marine planktonic thaumarchaeal isolates, Geochim. Cosmochim. Acta, 171, 238–255, https://doi.org/10.1016/j.gca.2015.09.004, 2015.

Elling, F. J., Könneke, M., Nicol, G. W., Stieglmeier, M., Bayer, B., Spieck, E., De La Torre, J. R., Becker, K. W., Thomm, M., Prosser, J. I., Herndl, G. J., Schleper, C., and Hinrichs, K.: Chemotaxonomic characterisation of the thaumarchaeal lipidome, Environ. Microbiol., 19, 2681–2700, https://doi.org/10.1111/1462-2920.13759, 2017.

Hingley, J. S., Martins, C. C., Walker-Trivett, C., Adams, J. K., Naeher, S., Häggi, C., Feakins, S. J., and Naafs, B. D. A.: The global distribution of Isoprenoidal Glycerol Dialkyl Diethers (isoGDDs) is consistent with a predominant degradation origin, Org. Geochem., 192, 104782, https://doi.org/10.1016/j.orggeochem.2024.104782, 2024.

Huguet, C., Fietz, S., and Rosell-Melé, A.: Global distribution patterns of hydroxy glycerol dialkyl glycerol tetraethers, Org.Geochem., 57, 107–118, https://doi.org/10.1016/j.orggeochem.2013.01.010, 2013.

Knappy, C. S. and Keely, B. J.: Novel glycerol dialkanol triols in sediments: transformation products of glycerol dibiphytanyl glycerol tetraether lipids or biosynthetic intermediates?, Chem. Commun., 48, 841–843, https://doi.org/10.1039/C1CC15841D, 2012.

Koga, Y., Nishihara, M., Morii, H., and Akagawa-Matsushita, M.: Ether Polar Lipids of Methanogenic Bacteria: Structures, Comparative Aspects, and Biosyntheses, Microbiol. Rev., 57, https://doi.org/10.1128/mr.57.1.164-182.199, 1993.

Liu, X., Summons, R. E., and Hinrichs, K.: Extending the known range of glycerol ether lipids in the environment: structural assignments based on tandem mass spectral fragmentation patterns, Rap. Comm. Mass Spectrom., 26, 2295–2302, https://doi.org/10.1002/rcm.6355, 2012a.

Liu, X.-L., Lipp, J. S., Simpson, J. H., Lin, Y.-S., Summons, R. E., and Hinrichs, K.-U.: Mono- and dihydroxyl glycerol dibiphytanyl glycerol tetraethers in marine sediments: Identification of both core and intact polar lipid forms, Geochim. Cosmochim. Acta, 89, 102–115, https://doi.org/10.1016/j.gca.2012.04.053, 2012b.

Lü, X., Liu, X.-L., Elling, F. J., Yang, H., Xie, S., Song, J., Li, X., Yuan, H., Li, N., and Hinrichs, K.-U.: Hydroxylated isoprenoid GDGTs in Chinese coastal seas and their potential as a paleotemperature proxy for mid-to-low latitude marginal seas, Org. Geochem., 89–90, 31–43, https://doi.org/10.1016/j.orggeochem.2015.10.004, 2015.

Meador, T. B., Zhu, C., Elling, F. J., Könneke, M., and Hinrichs, K.-U.: Identification of isoprenoid glycosidic glycerol dibiphytanol diethers and indications for their biosynthetic origin, Org.Geochem., 69, 70–75, https://doi.org/10.1016/j.orggeochem.2014.02.005, 2014.

Mitrović, D., Hopmans, E. C., Bale, N. J., Richter, N., Amaral-Zettler, L. A., Baxter, A. J., Peterse, F., Miguel Raposeiro, P., Gonçalves, V., Cristina Costa, A., and Schouten, S.: Isoprenoidal GDGTs and GDDs associated with anoxic lacustrine environments, Org. Geochem., 178, 104582, https://doi.org/10.1016/j.orggeochem.2023.104582, 2023.

Pancost, R. D., McClymont, E. L., Bingham, E. M., Roberts, Z., Charman, D. J., Hornibrook, E. R. C., Blundell, A., Chambers, F. M., Lim, K. L. H., and Evershed, R. P.: Archaeol as a methanogen biomarker in ombrotrophic bogs, Org.Geochem., 42, 1279–1287, https://doi.org/10.1016/j.orggeochem.2011.07.003, 2011.

Pitcher, A., Rychlik, N., Hopmans, E. C., Spieck, E., Rijpstra, W. I. C., Ossebaar, J., Schouten, S., Wagner, M., and Sinninghe Damsté, J. S.: Crenarchaeol dominates the membrane lipids of *Candidatus* Nitrososphaera gargensis, a thermophilic Group I.1b Archaeon, ISME J. 4, 542–552, https://doi.org/10.1038/ismej.2009.138, 2010.

Rossel, P. E., Lipp, J. S., Fredricks, H. F., Arnds, J., Boetius, A., Elvert, M., and Hinrichs, K.-U.: Intact polar lipids of anaerobic methanotrophic archaea and associated bacteria, Org. Geochem., 39, 992–999, https://doi.org/10.1016/j.orggeochem.2008.02.021, 2008.

Schouten, S., Hopmans, E. C., Pancost, R. D., and Damsté, J. S. S.: Widespread occurrence of structurally diverse tetraether membrane lipids: Evidence for the ubiquitous presence of low-temperature relatives of hyperthermophiles, Proc. Natl. Acad. Sci. U.S.A., 97, 14421–14426, https://doi.org/10.1073/pnas.97.26.14421, 2000.

Schouten, S., Hopmans, E. C., Schefuß, E., and Sinninghe Damsté, J. S.: Distributional variations in marine crenarchaeotal membrane lipids: a new tool for reconstructing ancient sea water temperatures?, Earth. Planet. Sci. Lett., 204, 265–274, https://doi.org/10.1016/S0012-821X(02)00979-2, 2002.

Schouten, S., Pitcher, A., Hopmans, E. C., Villanueva, L., Van Bleijswijk, J., and Sinninghe Damsté, J. S.: Intact polar and core glycerol dibiphytanyl glycerol tetraether lipids in the Arabian Sea oxygen minimum zone: I. Selective preservation and degradation in the water column and consequences for the TEX86, Geochim. Cosmochim. Acta, 98, 228–243, https://doi.org/10.1016/j.gca.2012.05.002, 2012.

Schouten, S., Hopmans, E. C., and Sinninghe Damsté, J. S.: The organic geochemistry of glycerol dialkyl glycerol tetraether lipids: A review, Org. Geochem., 54, 19–61, https://doi.org/10.1016/j.orggeochem.2012.09.006, 2013.

Schubotz, F., Wakeham, S. G., Lipp, J. S., Fredricks, H. F., and Hinrichs, K.: Detection of microbial biomass by intact polar membrane lipid analysis in the water column and surface sediments of the Black Sea, Environ. Microbiol., 11, 2720–2734, https://doi.org/10.1111/j.1462-2920.2009.01999.x, 2009.

Sinninghe Damsté, J. S., Rijpstra, W. I. C., Hopmans, E. C., Jung, M.-Y., Kim, J.-G., Rhee, S.-K., Stieglmeier, M., and Schleper, C.: Intact Polar and Core Glycerol Dibiphytanyl Glycerol Tetraether Lipids of Group I.1a and I.1b Thaumarchaeota in Soil, Appl. Environ. Microbiol., 78, 6866–6874, https://doi.org/10.1128/AEM.01681-12, 2012.

Sinninghe Damsté, J. S., Rijpstra, W. I. C., Hopmans, E. C., Den Uijl, M. J., Weijers, J. W. H., and Schouten, S.: The enigmatic structure of the crenarchaeol isomer, Org. Geochem., 124, 22–28, https://doi.org/10.1016/j.orggeochem.2018.06.005, 2018.

Sinninghe Damsté, J. S. S., Schouten, S., Hopmans, E. C., Van Duin, A. C. T., and Geenevasen, J. A. J.: Crenarchaeol, Journal of Lipid Research, 43, 1641–1651, https://doi.org/10.1194/jlr.M200148-JLR200, 2002.

Umoh, U. U., Li, L., Wang, J., Kauluma, N., Asuquo, F. E., and Akpan, E. R.: Glycerol dialkyl glycerol tetraether signatures in tropical mesotidal estuary sediments of Qua Iboe River, Gulf of Guinea, Org. Geochem., 170, 104461, https://doi.org/10.1016/j.orggeochem.2022.104461, 2022.

Varma, D., Hopmans, E. C., Van Kemenade, Z. R., Kusch, S., Berg, S., Bale, N. J., Sangiorgi, F., Reichart, G.-J., Sinninghe Damsté, J. S., and Schouten, S.: Evaluating isoprenoidal hydroxylated GDGT-based temperature proxies in surface sediments from the global ocean, Geochim. Cosmochim. Acta, 370, 113–127, https://doi.org/10.1016/j.gca.2023.12.019, 2024.

Villanueva, L., Schouten, S., and Sinninghe Damsté, J. S.: Depth-related distribution of a key gene of the tetraether lipid biosynthetic pathway in marine T haumarchaeota, Environ. Microbiol., 17, 3527–3539, https://doi.org/10.1111/1462-2920.12508, 2015.

Wakeham, S. G., Turich, C., Schubotz, F., Podlaska, A., Li, X. N., Varela, R., Astor, Y., Sáenz, J. P., Rush, D., Sinninghe Damsté, J. S., Summons, R. E., Scranton, M. I., Taylor, G. T., and Hinrichs, K.-U.: Biomarkers,

chemistry and microbiology show chemoautotrophy in a multilayer chemocline in the Cariaco Basin, Deep-Sea Res. I: Oceanogr. Res. Pap., 63, 133–156, https://doi.org/10.1016/j.dsr.2012.01.005, 2012.
Xie, S., Liu, X.-L., Schubotz, F., Wakeham, S. G., and Hinrichs, K.-U.: Distribution of glycerol ether lipids in the oxygen minimum zone of the Eastern Tropical North Pacific Ocean, Org. Geochem., 71, 60–71, https://doi.org/10.1016/j.orggeochem.2014.04.006, 2014.
Zeng, Z., Liu, X.-L., Farley, K. R., Wei, J. H., Metcalf, W. W., Summons, R. E., and Welander, P. V.: GDGT cyclization proteins identify the dominant archaeal sources of tetraether lipids in the ocean, Proc. Natl. Acad. Sci. U.S.A., 116, 22505–22511, https://doi.org/10.1073/pnas.1909306116, 2019.
Zhang, T., He, W., Liang, Q., Zheng, F., Xiao, X., Zeng, Z., Zhou, J., Yao, W., Chen, H., Zhu, Y., Zhao, J., Zheng, Y., and Zhang, C.: Lipidomic diversity and proxy implications of archaea from cold seep sediments of the South China Sea, Front. Microbiol., 14, 1241958, https://doi.org/10.3389/fmicb.2023.1241958, 2023.

S2. Supplemental Data

Table S1: Scotian Slope samples.

Sample name	Sample ID[a]	Sample type[b]	Core type	Lat.	Long.	Water depth (m)	Top core sample depth (cmbsf)	Bottom core sample depth (cmbsf)	$TOC_{predicted}$ (wt. %)	$TOC_{adjusted}$ (wt. %)	TN (wt. %)	$\delta^{13}C_{TOC}$ (‰)	Extracted sediment (g)	TLE (µg g^{-1} $sed.^{-1}$)	Hydrocarbon detection[c]
2015-1, 180*	NSPC-2015018-001-S01B	Mud	Piston	42.112938	-64.405270	2082	172	178	0.7	1.1	0.09	-	20.1	546	Ambient
2015-3, 490	NSPC-2015018-003-S03B	Mud	Piston	42.052693	-64.700207	2016	485	491	0.4	1.0	0.06	-	20.22	255	Ambient
2015-4, 600	NSPC-2015018-004-S04 B	Mud	Piston	42.310843	-63.886528	1763	594	599	-	-	-	-	20.31	176	Ambient
2015-6, 220	NSPC 2015018-0006 S01 B	Mud	Piston	41.927130	-63.716420	2648	220	226	0.7	1.3	0.07	-	20.14	251	Ambient
2015-6, 330	NSPC 2015018-0006 S02 B	Mud	Piston	41.927130	-63.716420	2648	328	333	0.7	1.3	0.07	-	20.29	375	
2015-6, 360	NSPC 2015018-0006 S03 B	Mud	Piston	41.927130	-63.716420	2648	360	365	0.4	0.9	0.04	-	20.4	302	
2015-6, 500	NSPC 2015018-0006 S04 B	Mud	Piston	41.927130	-63.716420	2648	500	505	0.5	1.1	0.07	-	20.19	822	
2015-8, 750*	NSPC-2015018-008-S03 B	Mud	Piston	42.097695	-63.693832	2360	739	744	0.1	0.8	0.06	-	20.74	358	Ambient
2016-1, 630	2016011-001 S03 B	Mud	Piston	41.724833	-64.796127	2533	631	636	0.3	0.9	0.03	-	20	185	Ambient
2016-3, 160	2016011-003 S01 B	Mud	Piston	41.804088	-64.869017	2376	160	165	0.4	0.8	0.09	-	20.18	144	Ambient
2016-12, 640	2016011-012 S03 B	Mud	Piston	42.293287	-63.997142	1760	640	645	0.4	1.1	0.09	-	20.08	222	Ambient
2016-14, 300*	2016011-014 S01 B	Mud	Piston	41.927357	-63.716940	2585	295	300	0.3	0.9	0.06	-	20.13	298	Ambient
2016-14, 380*	2016011-014 S02 B	Mud	Piston	41.927357	-63.716940	2585	375	380	0.5	1.0	0.04	-	20.06	170	
2016-14, 400*	2016011-014 S03 B	Mud	Piston	41.927357	-63.716940	2585	399	404	0.3	0.9	0.05	-	20.02	94	
2016-14, 580*	2016011-014 S04 B	Mud	Piston	41.927357	-63.716940	2585	573	578	-	-	-	-	20.09	114	
2016-14, 780*	2016011-014 S05 B	Mud	Piston	41.927357	-63.716940	2585	775	780	0.3	0.9	0.07	-	20.12	107	
2016-14, 870*	2016011-014 S06 B	Mud	Piston	41.927357	-63.716940	2585	871	876	0.2	0.8	0.05	-	20.05	100	
2015-9, 150	NSPC 2015018-0009 S01 B	Mud	Piston	42.308610	-62.836325	2284	144	149	0.5	0.9	0.05	-	20.73	123	Ambient
2015-9, 300	NSPC 2015018-0009 S03 B	Mud	Piston	42.308610	-62.836325	2284	297	302	0.4	0.9	0.06	-	20.95	437	
2015-9, 370	NSPC 2015018-0009 S04 B	Mud	Piston	42.308610	-62.836325	2284	363	369	0.4	1.0	0.02	-	20.52	500	
2015-11, 350	NSPC-2015018-011-S03 B	Mud	Piston	42.270058	-62.938060	2327	346	351	0.4	0.9	0.05	-	20.57	245	Ambient
2015-12, 700	NSPC-2015018-012-S03 B	Mud	Piston	42.321158	-62.467133	2324	700	705	0.5	1.2	0.1	-	20.15	154	Ambient
2015-13, 700*	NSPC-2015018-013-S03 B	Mud	Piston	42.360212	-62.465482	2208	698	704	0.3	0.9	0.08	-	20.3	123	Ambient
2016-15, 690	2016011-015 S04 B	Mud	Piston	42.305998	-63.243618	2050	684	694	-	-	-	-	20.05	136	Ambient
2016-17, 470	2016011-017 S03 B	Mud	Piston	42.228892	-63.117570	2315	463	468	0.3	0.9	0.04	-	20.1	232	Ambient
2016-20, 720	2016011-020 S03 B	Mud	Piston	42.304433	-62.685662	2190	718	723	0.3	0.9	0.08	-	20.95	158	Ambient
2016-22, 600	2016011-022 S03 B	Mud	Piston	42.009998	-62.814178	2822	598	603	0.4	1.0	0.09	-	20.42	95	Ambient
2016-24, 700	2016011-024 S02 B	Mud	Piston	41.878680	-62.837250	3095	695	700	0.3	0.9	0.1	-	20.04	99	Ambient
2016-25, 270	2016011-025 S01 B	Mud	Piston	42.053920	-62.518298	2880	267	272	0.3	0.8	0.05	-	21.45	132	Ambient
2016-25, 290	2016011-025 S02 B	Mud	Piston	42.053920	-62.518298	2880	287	292	0.2	0.8	0.03	-	20	375	
2016-25, 300	2016011-025 S03 B	Mud	Piston	42.053920	-62.518298	2880	301	306	0.3	0.9	0.07	-	20	280	
2016-25, 800	2016011-025 S04 B	Mud	Piston	42.053920	-62.518298	2880	791	796	0.4	1.0	0.1	-	20.16	492	
2016-26, 490	2016011-026 S02 B	Mud	Piston	42.104218	-62.538445	2760	483	488	0.4	1.0	0.07	-	20	152	Ambient
2016-28, 660	2016011-028 S02 B	Mud	Piston	42.279317	-62.310168	2510	655	660	0.3	0.9	0.09	-	20.07	229	Ambient
2016-29, 700	2016011-029 S03 B	Mud	Piston	42.196683	-62.313510	2730	704	709	0.5	1.2	0.07	-	20	421	Ambient
2016-30, 630	2016011-030 S02 B	Mud	Piston	42.470058	-62.130127	2106	630	635	0.3	0.9	0.09	-	20.17	146	Ambient
2016-49, 450	2016011-049 S06 B	Mud	Piston	42.159815	62.359747	2715	443	448	0.5	1.0	0	-	20.18	217	Ambient
2018-21, 0	2018041-0021 gc	Mud	Gravity	42.494195	-62.126415	2079	5	10	0.7	0.9	0.1	-	22.01	177	Ambient
2018-21, 60	2018041-0021 gc	Mud	Gravity	42.494195	-62.126415	2079	55	60	0.5	0.8	0.07	-	20	547	
2018-21, 140	2018041-0021 gc	Mud	Gravity	42.494195	-62.126415	2079	140	145	0.5	0.9	0.08	-	20.43	500	
2018-21, 210	2018041-0021 gc	Mud	Gravity	42.494195	-62.126415	2079	210	217	0.4	0.9	0.05	-	20.55	128	
2018-21, 240	2018041-0021 gc	Mud	Gravity	42.494195	-62.126415	2079	236	241	0.4	0.9	0.07	-	20.06	187	
2018-21, 320	2018041-0021 gc	Mud	Gravity	42.494195	-62.126415	2079	312	317	0.5	1.1	0.05	-	20.03	108	
2018-21, 410	2018041-0021 gc	Mud	Gravity	42.494195	-62.126415	2079	405	410	0.2	0.8	0.05	-	20.3	324	
2018-21, 450	2018041-0021 gc	Mud	Gravity	42.494195	-62.126415	2079	446	451	0.2	0.8	0.05	-	20.13	144	
2018-21, 520	2018041-0021 gc	Mud	Gravity	42.494195	-62.126415	2079	514	520	0.2	0.8	0.04	-	20.03	247	
2018-21, 570	2018041-0021 gc	Mud	Gravity	42.494195	-62.126415	2079	565	570	0.3	0.9	0.05	-	20.27	148	
2018-21, 610	2018041-0021 gc	Mud	Gravity	42.494195	-62.126415	2079	610	615	0.3	0.9	0.07	-	20.04	168	
2018-21, 670	2018041-0021 gc	Mud	Gravity	42.494195	-62.126415	2079	667	672	0.3	0.9	0.07	-	20.21	146	

2018-21, 710	2018041-0021 gc	Mud	Gravity	42.494195	-62.126415	2079	710	715	0.3	0.9	0.06	-	20.03	182	
2018-22, 0	2018041-0022 gc	Mud	Gravity	42.492181	-62.128928	2083	0	5	0.7	0.9	0.09	-21.74	20.05	296	Ambient
2018-22, 60	2018041-0022 gc	Mud	Gravity	42.492181	-62.128928	2083	52	60	0.6	0.9	0.08	-	20.04	504	
2018-22, 110	2018041-0022 gc	Mud	Gravity	42.492181	-62.128928	2083	110	115	0.6	1.0	0.06	-22.74	20.15	280	
2018-22, 150	2018041-0022 gc	Mud	Gravity	42.492181	-62.128928	2083	151	156	0.4	0.8	0.02	-	21.91	131	
2018-22, 270	2018041-0022 gc	Mud	Gravity	42.492181	-62.128928	2083	268	273	0.4	0.9	0.06	-23.73	20.01	125	
2018-22, 300	2018041-0022 gc	Mud	Gravity	42.492181	-62.128928	2083	301	309	0.4	1.0	0.04	-	20.5	309	
2018-22, 360	2018041-0022 gc	Mud	Gravity	42.492181	-62.128928	2083	360	365	0.4	1.0	0.07	-22.87	20.42	161	
2018-22, 410	2018041-0022 gc	Mud	Gravity	42.492181	-62.128928	2083	409	414	0.2	0.8	0.04	-23.17	20.09	141	
2018-22, 460	2018041-0022 gc	Mud	Gravity	42.492181	-62.128928	2083	460	466	0.3	0.9	0.04	-23.89	20.13	135	
2018-23, 0	2018041-0023 gc	Mud	Gravity	42.466221	-62.192356	2154	5	10	0.7	0.9	0.1	-21.77	20.02	146	Ambient
2018-23, 40	2018041-0023 gc	Mud	Gravity	42.466221	-62.192356	2154	35	40	0.6	0.9	0.09	-	20.69	192	
2018-23, 100	2018041-0023 gc	Mud	Gravity	42.466221	-62.192356	2154	92	98	0.5	0.9	0.07	-22.31	20.74	195	
2018-23, 130	2018041-0023 gc	Mud	Gravity	42.466221	-62.192356	2154	125	130	0.5	0.9	0.07	-	20.8	986	
2018-23, 200	2018041-0023 gc	Mud	Gravity	42.466221	-62.192356	2154	192	198	0.6	1.1	0.08	-22.26	20	355	
2018-23, 220	2018041-0023 gc	Mud	Gravity	42.466221	-62.192356	2154	220	225	0.7	1.2	0.08	-	20.12	242	
2018-23, 280	2018041-0023 gc	Mud	Gravity	42.466221	-62.192356	2154	272	286	0.5	1.0	0.05	-23.83	20.15	399	
2018-23, 340	2018041-0023 gc	Mud	Gravity	42.466221	-62.192356	2154	335	340	0.5	1.0	0.07	-24.38	20.09	354	
2015-16, 620	NSPC-2015018-016-S04 B	Mud	Piston	42.774882	-61.234878	2233	614	619	0.4	1.0	0.09	-	20.2	168	Ambient
2016-38, 570	2016011-038 S03 B	Mud	Piston	42.862812	-60.844940	2250	563	568	0.4	1.0	0.1	-	20.31	148	Ambient
2015-24, 600	NSPC-2015018-024-S04 B	Mud	Piston	43.340303	-59.958477	1540	594	599	1.1	1.7	0.11	-	20.9	743	Ambient
2015-29, 500	NSPC-2015018-029-S03 B	Mud	Piston	43.270203	-60.058940	1620	490	495	0.8	1.4	0.12	-	20.28	560	Ambient
2018-07, 0	2018041-0007 gc	Mud	Gravity	43.010485	-60.211696	2405	0	4	0.1	0.4	0.02	-21.97	20.15	121	Seep
2018-07, 20	2018041-0007 gc	Mud	Gravity	43.010485	-60.211696	2405	18	24	0.3	0.5	0.05	-27.43	20.08	202	
2018-07, 40	2018041-0007 gc-Isojar	Isojar	Gravity	43.010485	-60.211696	2405	26	42	0.3	0.6	0.05	-22.87	22.02	207	

[*] Core to which one to two radiocarbon age dates were recorded (Jenner et al., 2022). Radiocarbon age dates from Jenner et al. totaled 9 dates from 7 cores (two dates from two cores were not sampled in our study).

[a] Cores are labelled by the year of the cruise, followed by core number, core site number.

[b] Sediment type is sourced from open file cruise reports (Campbell and MacDonald, 2016; Campbell, 2019; and Campbell and Normandeau, 2019).

[c] Determination of hydrocarbon input is provided by Fowler et at. (2017).

Table S2: Lithological information of Scotian Slope samples.

Sample name	Sample ID[a]	Lat.	Long.	Sediment colour, texture, and lithology[b]
2015-1, 180	NSPC-2015018-001-S01B	42.112938	-64.405270	Reddish brown mud
2015-3, 490	NSPC-2015018-003-S03B	42.052693	-64.700207	Greyish brown mud with sand laminations and lenses
2015-4, 600	NSPC-2015018-004-S04 B	42.310843	-63.886528	Greyish brown mud with sand laminations and lenses
2015-6, 220	NSPC 2015018-0006 S01 B	41.927130	-63.716420	Greyish brown mud with sand laminations
2015-6, 330	NSPC 2015018-0006 S02 B	41.927130	-63.716420	Grey mud with sand laminations
2015-6, 360	NSPC 2015018-0006 S03 B	41.927130	-63.716420	Grey mud with sand laminations
2015-6, 500	NSPC 2015018-0006 S04 B	41.927130	-63.716420	Reddish brown mud with sand laminations
2015-8, 750	NSPC-2015018-008-S03 B	42.097695	-63.693832	Reddish brown mud with sand laminations
2016-1, 630	2016011-001 S03 B	41.724833	-64.796127	Dark grey mud with coarse sand laminations
2016-3, 160	2016011-003 S01 B	41.804088	-64.869017	Dark grey mud with sparse sand
2016-12, 640	2016011-012 S03 B	42.293287	-63.997142	Dark grey mud with sand laminations
2016-14, 300	2016011-014 S01 B	41.927357	-63.716940	Dark grey silty clay with fine sand laminations
2016-14, 380	2016011-014 S02 B	41.927357	-63.716940	Reddish brown silty clay with fine sand laminations
2016-14, 400	2016011-014 S03 B	41.927357	-63.716940	Dark grey silty clay with sand laminations
2016-14, 580	2016011-014 S04 B	41.927357	-63.716940	Dark grey silty clay with sand laminations
2016-14, 780	2016011-014 S05 B	41.927357	-63.716940	Reddish brown mud with gradual transition to dark grey and sand laminations
2016-14, 870	2016011-014 S06 B	41.927357	-63.716940	Dark grey silty clay with very fine sand laminations
2015-9, 150	NSPC 2015018-0009 S01 B	42.308610	-62.836325	Grey mud
2015-9, 300	NSPC 2015018-0009 S03 B	42.308610	-62.836325	Grey mud with sand lenses
2015-9, 370	NSPC 2015018-0009 S04 B	42.308610	-62.836325	Greyish brown mud clast conglomerate
2015-11, 350	NSPC-2015018-011-S03 B	42.270058	-62.938060	Greyish brown mud with sand laminations
2015-12, 700	NSPC-2015018-012-S03 B	42.321158	-62.467133	Greyish brown mud
2015-13, 700	NSPC-2015018-013-S03 B	42.360212	-62.465482	Greenish brown mud
2016-15, 690	2016011-015 S04 B	42.305998	-63.243618	Greyish brown mud with transition to reddish brown and fine sand laminations
2016-17, 470	2016011-017 S03 B	42.228892	-63.117570	Reddish brown silty clay with coarse sand laminations
2016-20, 720	2016011-020 S03 B	42.304433	-62.685662	Dark grey silty clay with transition to reddish brown and sand laminations
2016-22, 600	2016011-022 S03 B	42.009998	-62.814178	Dark grey silty clay with coarse sand laminations
2016-24, 700	2016011-024 S02 B	41.878680	-62.837250	Reddish grey silty clay with fine sand lenses
2016-25, 270	2016011-025 S01 B	42.053920	-62.518298	Greyish brown silty clay with fine sand laminations
2016-25, 290	2016011-025 S02 B	42.053920	-62.518298	Greyish brown silty clay with fine sand lenses
2016-25, 300	2016011-025 S03 B	42.053920	-62.518298	Greyish brown silty clay with sand laminations
2016-25, 800	2016011-025 S04 B	42.053920	-62.518298	Reddish brown silty clay with sand laminations
2016-26, 490	2016011-026 S02 B	42.104218	-62.538445	Greyish brown silty clay with sand laminations
2016-28, 660	2016011-028 S02 B	42.279317	-62.310168	Reddish brown silty clay with fine sand lenses
2016-29, 700	2016011-029 S03 B	42.196683	-62.313510	Dark grey silty clay with fine sand lenses and laminations
2016-30, 630	2016011-030 S02 B	42.470058	-62.130127	Greyish brown silty clay with fine sand lenses
2016-49, 450	2016011-049 S06 B	42.159815	62.359747	Greenish grey silty clay
2018-21, 0	2018041-0021 gc	42.494195	-62.126415	Dark grey silty clay
2018-21, 60	2018041-0021 gc	42.494195	-62.126415	Dark grey silty clay
2018-21, 140	2018041-0021 gc	42.494195	-62.126415	Brown silty clay
2018-21, 210	2018041-0021 gc	42.494195	-62.126415	Brown silty clay
2018-21, 240	2018041-0021 gc	42.494195	-62.126415	Brown silty clay
2018-21, 320	2018041-0021 gc	42.494195	-62.126415	Brown silty clay
2018-21, 410	2018041-0021 gc	42.494195	-62.126415	Reddish brown clay
2018-21, 450	2018041-0021 gc	42.494195	-62.126415	Dark reddish grey silty clay
2018-21, 520	2018041-0021 gc	42.494195	-62.126415	Dark reddish grey silty clay
2018-21, 570	2018041-0021 gc	42.494195	-62.126415	Dark grey silty clay
2018-21, 610	2018041-0021 gc	42.494195	-62.126415	Brown silty clay
2018-21, 670	2018041-0021 gc	42.494195	-62.126415	Dark grey silty clay
2018-21, 710	2018041-0021 gc	42.494195	-62.126415	Dark grey silty clay
2018-22, 0	2018041-0022 gc	42.492181	-62.128928	Brown silty clay
2018-22, 60	2018041-0022 gc	42.492181	-62.128928	Greyish brown silty clay
2018-22, 110	2018041-0022 gc	42.492181	-62.128928	Dark grey silty clay
2018-22, 150	2018041-0022 gc	42.492181	-62.128928	Dark grey silty clay
2018-22, 270	2018041-0022 gc	42.492181	-62.128928	Dark grey silty clay
2018-22, 300	2018041-0022 gc	42.492181	-62.128928	Dark reddish brown silty clay
2018-22, 360	2018041-0022 gc	42.492181	-62.128928	Dark reddish brown silty clay
2018-22, 410	2018041-0022 gc	42.492181	-62.128928	Dark reddish brown silty clay
2018-22, 460	2018041-0022 gc	42.492181	-62.128928	Dark reddish brown silty clay

2018-23, 0	2018041-0023 gc	42.466221	-62.192356	Greyish brown silty clay with fine sand laminations
2018-23, 40	2018041-0023 gc	42.466221	-62.192356	Greyish brown silty clay with fine sand laminations
2018-23, 100	2018041-0023 gc	42.466221	-62.192356	Greyish brown silty clay with fine sand laminations
2018-23, 130	2018041-0023 gc	42.466221	-62.192356	Greyish brown silty clay with fine sand laminations
2018-23, 200	2018041-0023 gc	42.466221	-62.192356	Very dark greyish brown silty clay
2018-23, 220	2018041-0023 gc	42.466221	-62.192356	Dark grey silty clay
2018-23, 280	2018041-0023 gc	42.466221	-62.192356	Brownish grey mud with sand laminations
2018-23, 340	2018041-0023 gc	42.466221	-62.192356	Dark grey silty clay
2015-16, 620	NSPC-2015018-016-S04 B	42.774882	-61.234878	Brownish grey mud with sand laminations
2016-38, 570	2016011-038 S03 B	42.862812	-60.844940	Reddish brown silty clay with fine sand lenses
2015-24, 600	NSPC-2015018-024-S04 B	43.340303	-59.958477	Greyish brown mud
2015-29, 500	NSPC-2015018-029-S03 B	43.270203	-60.058940	Brown mud with sand laminations
2018-07, 0	2018041-0007 gc	43.010485	-60.211696	Light brownish grey silty sandy clay
2018-07, 20	2018041-0007 gc	43.010485	-60.211696	Dark grey massive silty clay
2018-07, 40	2018041-0007 gc-Isojar	43.010485	-60.211696	Greenish grey clay

[a] Cores are labelled by the year of the cruise, followed by core number, core site number.

[b] Lithologic information is extracted from open file cruise report Jenner et al. (2022) for cores collected on 2015 expedition cruise, and are provided by GSC Atlantic, NRCAN for cores collected on 2016 and 2018 expedition cruises.

Table S3: Detected archaeal IPLs and CLs, and upper water column photosynthetic pigments from Scotian Slope.

Chemical name	Abbreviation	RT (min)	Neutral mass	Diagnostic fragment ions	References
Monoglycosidic glycerol dialkyl glycerol tetraether	1G-GDGTs (0–3, and Cren)	45-47	1463.4, 1461.4, 1459.3, 1457.3, 1455.3, 1453.3	1302.3, 743.7, 651.7	Sturt et al., 2004
Diglycosidic glycerol dialkyl glycerol tetraether	2G-GDGTs (0–3)	40-42	1626.4, 1624.2, 1622.4, 1620.4, 1618.4, 1616.4	1302.3, 743.7, 651.7	Sturt et al., 2004; Meador et al., 2014
Hydroxyl monoglycosidic glycerol dialkyl glycerol tetraether	1G-OH-GDGTs (0–2)	38-39	1479.4, 1477.3, 1475.3, 1473.3, 1471.3, 1469.3	1318.3, 760.7, 668.7	Lipp and Hinrichs, 2009; Liu et al., 2012c
Hydroxyl diglycosidic glycerol dialkyl glycerol tetraether	2G-OH-GDGTs (0–2)	34-36	1641.4, 1639.4, 1637.4, 1635.4, 1633.4, 1631.3	1318.3, 760.7, 668.7	Lipp and Hinrichs, 2009; Liu et al., 2012c
Monoglycosidic archaeol	1G-AR	14	814.8	653, 373	Lipp and Hinrichs, 2009; Yoshinaga et al., 2011
Diglycosidic archaeol	2G-AR	11	976.8	653, 373	Lipp and Hinrichs, 2009; Yoshinaga et al., 2011
Phosphatidicacid archaeol	PA-AR	9	732.6	453.3, 357.4	Yoshinaga et al., 2011
Hydroxyphosphatidicacid archaeol	PA-OH-AR	4-5	748.6	453.3	Yoshinaga et al., 2011
Isoprenoidal glycerol dialkyl glycerol tetraether	GDGTs (0–3, Cren, and Cren´)	54-57	1301.3, 1299.3, 1297.3, 1295.3, 1293.3, 1291.3	1302.3, 743.7, 651.7	Hopmans et al., 2000; Schouten et al., 2013; Sinninghe Damsté et al., 2002
Hydroxyl glycerol dialkyl glycerol tetraether	OH-GDGTs (0–2)	44-46	1317.3, 1315.3, 1313.3, 1311.3, 1309.2, 1307.2	1302.3, 743.7, 651.7	Liu et al., 2012a
Glycerol dialkanol diether	GDDs (0–4, and Cren)	41-44	1245.3, 1243.3, 1241.3, 1239.2, 1237.2, 1235.2	669.6	Liu et al., 2012a; Liu et al., 2012b
Hydroxylated glycerol dialkanol diether	OH-GDDs (0–2)	33-34	1261.3, 1259.3, 1257.3, 1255.2, 1253.2, 1251.2	686.6	Liu et al., 2012a; Liu et al., 2012b
Archaeol	AR	19	652.7	373.3	Lipp and Hinrichs, 2009; Yoshinaga et al., 2011
Biphytanic diol	BpDiols (0–3)	12	594.6, 592.6, 590.6, 588.6	549.5	Liu et al., 2012a; Liu et al., 2012b
Chlorophyll *a*	Chl-*a*	17-18	892.5	593.3, 533.5	Chen et al., 2015; Milenkovic et al., 2012
Hydroxychlorophyll *a*	OH-Chl-*a*	14-15	908.5	593.3, 533.5	Chen et al., 2015

Quantification of IPLs and CLs was achieved by merging the integrated peak areas of $[M^{\cdot}+H]^+$, $[M^{\cdot}+NH_4]^+$, and $[M^{\cdot}+Na]^+$ adduct ions.

Table S4: Modelled TOC decay rate and pre-diagenesis scaling values for various burial depths (Eq. 2, 4, and 5).

y_i (mbsf)	$\mathrm{TOC}_{predicted_i}$ (wt. %) Eq. (3)	n_i Eq. (4)	$\mathrm{TOC}_{decayed_i}$ (wt. %) Eq. (5)
0	1.1	NA	NA
1	0.9	-0.24	0.3
2	0.7	-0.18	0.4
3	0.5	-0.14	0.5
4	0.4	-0.10	0.6
5	0.3	-0.08	0.6
6	0.2	-0.06	0.6
7	0.2	-0.05	0.6
8	0.1	-0.03	0.6
9	0.1	-0.03	0.6

Table S5: Concentration of ARs, upper water column photosynthetic pigments, and archaeal IPLs in Scotian Slope sediments.

Sample name	1G-GDGT					1G-OH-GDGT			2G-GDGT			2G-OH-GDGT			ARs					Upper water column photosynthetic pigments	
	1G-GDGT-0	1G-GDGT-1	1G-GDGT-2	1G-GDGT-3	1G-GDGT-5	1G-OH-GDGT-0	1G-OH-GDGT-1	1G-OH-GDGT-2	2G-GDGT-O	2G-GDGT-1	2G-GDGT-2	2G-OH-GDGT-0	2G-OH-GDGT-1	2G-OH-GDGT-2	AR	1G-AR	2G-AR	PA-AR	PA-OH-AR	Chl-*a*	OH-Chl-*a*
2015-1, 180	0.027	0.004	0.003	0.001	0.023	0.006	0.003	0.000	0.006	0.003	0.002	0.011	0.005	0.001	0.044	0.000	0.003	0.181	0.000	0.002	0.000
2015-3, 490	0.053	0.005	0.003	0.000	0.049	0.012	0.005	0.000	0.006	0.004	0.002	0.012	0.008	0.001	0.106	0.002	0.009	0.093	0.017	0.010	0.000
2015-4, 600	0.063	0.006	0.004	0.001	0.059	0.017	0.008	0.001	0.007	0.004	0.001	0.016	0.010	0.002	0.134	0.002	0.009	0.114	0.030	0.004	0.000
2015-6, 220	0.035	0.006	0.007	0.001	0.034	0.008	0.004	0.000	0.006	0.003	0.002	0.011	0.006	0.001	0.208	0.000	0.010	0.262	0.000	0.004	0.000
2015-6, 330	0.037	0.004	0.005	0.001	0.031	0.007	0.002	0.000	0.006	0.003	0.002	0.013	0.007	0.002	0.057	0.000	0.000	0.320	0.000	0.006	0.000
2015-6, 360	0.061	0.006	0.001	0.000	0.053	0.010	0.005	0.000	0.004	0.002	0.001	0.012	0.007	0.001	0.233	0.000	0.017	0.073	0.000	0.003	0.000
2015-6, 500	0.056	0.005	0.004	0.001	0.042	0.014	0.004	0.000	0.003	0.002	0.000	0.011	0.006	0.001	0.135	0.003	0.011	0.067	0.000	0.000	0.000
2015-8, 750	0.076	0.005	0.001	0.000	0.062	0.016	0.006	0.000	0.002	0.002	0.001	0.011	0.008	0.001	0.051	0.002	0.007	0.157	0.000	0.012	0.000
2016-1, 630	0.106	0.008	0.004	0.001	0.088	0.023	0.007	0.002	0.004	0.003	0.002	0.015	0.008	0.002	0.272	0.001	0.001	0.000	0.000	0.000	0.004
2016-3, 160	0.074	0.007	0.003	0.000	0.064	0.017	0.007	0.001	0.003	0.002	0.001	0.013	0.009	0.002	0.299	0.001	0.001	0.000	0.000	0.000	0.000
2016-12, 640	0.148	0.011	0.007	0.001	0.123	0.020	0.008	0.002	0.003	0.002	0.000	0.008	0.005	0.001	0.370	0.001	0.020	0.001	0.000	0.009	0.000
2016-14, 300	0.250	0.020	0.014	0.001	0.215	0.031	0.013	0.002	0.006	0.005	0.003	0.021	0.011	0.001	0.408	0.001	0.048	0.000	0.000	0.046	0.000
2016-14, 380	0.093	0.007	0.004	0.000	0.071	0.018	0.008	0.001	0.002	0.001	0.001	0.012	0.007	0.001	0.389	0.000	0.015	0.000	0.000	0.005	0.000
2016-14, 400	0.078	0.006	0.005	0.001	0.057	0.016	0.008	0.002	0.002	0.002	0.000	0.009	0.005	0.001	0.277	0.001	0.009	0.000	0.000	0.009	0.000
2016-14, 580	0.093	0.007	0.006	0.001	0.074	0.016	0.008	0.002	0.002	0.001	0.000	0.011	0.006	0.006	0.331	0.001	0.011	0.000	0.000	0.006	0.000
2016-14, 780	0.070	0.009	0.006	0.001	0.079	0.021	0.010	0.003	0.003	0.002	0.001	0.011	0.006	0.001	0.348	0.000	0.012	0.000	0.000	0.000	0.003
2016-14, 870	0.127	0.012	0.007	0.002	0.117	0.029	0.014	0.004	0.003	0.003	0.002	0.015	0.009	0.002	0.574	0.001	0.015	0.000	0.000	0.000	0.004
2015-9, 150	0.037	0.003	0.001	0.000	0.045	0.012	0.003	0.000	0.004	0.003	0.002	0.011	0.005	0.000	0.021	0.001	0.002	0.160	0.000	0.007	0.000
2015-9, 300	0.041	0.003	0.001	0.000	0.042	0.013	0.006	0.001	0.005	0.005	0.003	0.013	0.007	0.002	0.047	0.000	0.018	0.231	0.000	0.004	0.000
2015-9, 370	0.041	0.005	0.002	0.000	0.052	0.016	0.006	0.000	0.007	0.004	0.002	0.015	0.008	0.001	0.052	0.000	0.004	0.205	0.000	0.000	0.000
2015-11, 350	0.055	0.007	0.004	0.001	0.062	0.043	0.016	0.003	0.010	0.005	0.005	0.028	0.014	0.003	0.208	0.000	0.006	0.142	0.000	0.000	0.000
2015-12, 700	0.076	0.011	0.003	0.000	0.118	0.016	0.005	0.000	0.007	0.005	0.004	0.019	0.013	0.002	0.073	0.001	0.005	0.207	0.000	0.005	0.000
2015-13, 700	0.063	0.007	0.002	0.000	0.076	0.015	0.004	0.000	0.006	0.004	0.004	0.018	0.010	0.002	0.044	0.001	0.002	0.158	0.000	0.006	0.000
2016-15, 690	0.118	0.008	0.006	0.001	0.082	0.021	0.007	0.002	0.003	0.002	0.001	0.011	0.005	0.001	0.249	0.001	0.013	0.000	0.000	0.007	0.000
2016-17, 470	0.162	0.012	0.005	0.001	0.131	0.035	0.012	0.002	0.005	0.003	0.002	0.018	0.008	0.001	0.200	0.001	0.002	0.000	0.000	0.000	0.000
2016-20, 720	0.067	0.005	0.002	0.000	0.041	0.016	0.006	0.001	0.004	0.003	0.002	0.015	0.009	0.002	0.080	0.000	0.001	0.000	0.000	0.003	0.000
2016-22, 600	0.111	0.007	0.003	0.001	0.108	0.020	0.007	0.001	0.005	0.004	0.004	0.018	0.011	0.002	0.107	0.000	0.001	0.000	0.000	0.000	0.005
2016-24, 700	0.182	0.010	0.003	0.000	0.134	0.026	0.006	0.001	0.006	0.004	0.003	0.022	0.013	0.002	0.242	0.001	0.001	0.000	0.000	0.000	0.003
2016-25, 270	0.097	0.009	0.008	0.002	0.063	0.024	0.009	0.002	0.004	0.003	0.002	0.016	0.008	0.002	0.175	0.001	0.004	0.000	0.000	0.005	0.000
2016-25, 290	0.201	0.019	0.013	0.004	0.144	0.032	0.013	0.002	0.006	0.005	0.002	0.021	0.010	0.000	0.318	0.003	0.006	0.015	0.000	0.032	0.000
2016-25, 300	0.089	0.009	0.009	0.004	0.064	0.016	0.008	0.003	0.005	0.004	0.002	0.019	0.011	0.002	0.372	0.001	0.010	0.000	0.000	0.014	0.000
2016-25, 800	0.080	0.008	0.003	0.001	0.077	0.022	0.007	0.001	0.006	0.004	0.003	0.022	0.011	0.002	0.197	0.000	0.003	0.000	0.000	0.008	0.002
2016-26, 490	0.059	0.008	0.004	0.001	0.082	0.025	0.008	0.002	0.008	0.005	0.004	0.027	0.013	0.003	0.171	0.001	0.002	0.000	0.000	0.000	0.002
2016-28, 660	0.047	0.005	0.004	0.000	0.059	0.012	0.003	0.001	0.002	0.002	0.001	0.009	0.004	0.001	0.369	0.000	0.004	0.000	0.000	0.000	0.000
2016-29, 700	0.084	0.009	0.007	0.001	0.089	0.016	0.004	0.001	0.003	0.002	0.002	0.013	0.006	0.001	0.342	0.000	0.003	0.000	0.000	0.000	0.002
2016-30, 630	0.167	0.010	0.004	0.001	0.195	0.034	0.007	0.001	0.007	0.004	0.003	0.037	0.017	0.003	0.388	0.001	0.006	0.000	0.000	0.001	0.004
2016-49, 450	0.058	0.007	0.008	0.001	0.048	0.011	0.005	0.002	0.001	0.001	0.000	0.006	0.002	0.000	1.946	0.000	0.009	0.000	0.000	0.001	0.000

2018-21, 0	0.160	0.013	0.004	0.001	0.140	0.020	0.004	0.000	0.010	0.008	0.006	0.023	0.017	0.005	0.093	0.000	0.004	0.153	0.000	0.019	0.000
2018-21, 60	0.240	0.022	0.009	0.001	0.215	0.035	0.008	0.000	0.018	0.017	0.015	0.036	0.027	0.007	0.053	0.000	0.009	0.156	0.000	0.009	0.000
2018-21, 140	0.097	0.008	0.004	0.001	0.090	0.022	0.006	0.000	0.010	0.008	0.006	0.024	0.014	0.003	0.028	0.000	0.002	0.150	0.000	0.003	0.000
2018-21, 210	0.035	0.005	0.002	0.000	0.065	0.017	0.005	0.000	0.005	0.003	0.002	0.014	0.007	0.001	0.038	0.001	0.002	0.138	0.000	0.005	0.000
2018-21, 240	0.094	0.009	0.005	0.001	0.092	0.017	0.006	0.000	0.006	0.004	0.002	0.017	0.010	0.003	0.080	0.001	0.005	0.269	0.000	0.005	0.000
2018-21, 320	0.030	0.003	0.002	0.000	0.033	0.010	0.003	0.000	0.005	0.004	0.003	0.015	0.007	0.001	0.047	0.001	0.002	0.194	0.000	0.004	0.000
2018-21, 410	0.113	0.009	0.003	0.000	0.105	0.024	0.006	0.000	0.006	0.005	0.002	0.021	0.011	0.003	0.087	0.001	0.003	0.271	0.000	0.003	0.000
2018-21, 450	0.071	0.006	0.002	0.000	0.071	0.014	0.003	0.000	0.003	0.002	0.001	0.011	0.006	0.001	0.092	0.001	0.005	0.219	0.000	0.002	0.000
2018-21, 520	0.126	0.015	0.004	0.000	0.144	0.028	0.010	0.000	0.010	0.010	0.005	0.032	0.019	0.005	0.102	0.002	0.004	0.654	0.000	0.008	0.000
2018-21, 570	0.098	0.008	0.003	0.000	0.122	0.024	0.007	0.000	0.005	0.004	0.002	0.016	0.010	0.002	0.060	0.000	0.002	0.289	0.000	0.007	0.000
2018-21, 610	0.056	0.006	0.002	0.000	0.077	0.010	0.003	0.000	0.005	0.002	0.002	0.012	0.009	0.002	0.044	0.002	0.001	0.139	0.000	0.005	0.000
2018-21, 670	0.028	0.002	0.001	0.000	0.031	0.003	0.001	0.000	0.001	0.001	0.000	0.005	0.003	0.000	0.029	0.001	0.002	0.023	0.000	0.000	0.000
2018-21, 710	0.065	0.006	0.002	0.000	0.079	0.012	0.003	0.000	0.004	0.003	0.001	0.013	0.008	0.002	0.058	0.001	0.002	0.131	0.000	0.004	0.000
2018-22, 0	0.208	0.019	0.007	0.001	0.216	0.027	0.008	0.000	0.011	0.011	0.010	0.027	0.022	0.005	0.110	0.001	0.002	0.193	0.000	0.014	0.000
2018-22, 60	0.094	0.012	0.006	0.001	0.160	0.028	0.008	0.000	0.016	0.012	0.010	0.031	0.020	0.004	0.063	0.001	0.004	0.252	0.000	0.009	0.000
2018-22, 110	0.052	0.007	0.004	0.001	0.086	0.019	0.005	0.000	0.009	0.007	0.005	0.021	0.011	0.002	0.046	0.000	0.002	0.301	0.000	0.006	0.000
2018-22, 150	0.056	0.009	0.008	0.002	0.070	0.015	0.006	0.000	0.002	0.002	0.002	0.008	0.004	0.001	0.106	0.000	0.004	0.168	0.000	0.007	0.000
2018-22, 270	0.067	0.008	0.002	0.001	0.082	0.017	0.006	0.000	0.006	0.004	0.003	0.017	0.008	0.000	0.103	0.001	0.003	0.241	0.000	0.008	0.002
2018-22, 300	0.091	0.011	0.009	0.002	0.119	0.018	0.007	0.000	0.006	0.005	0.004	0.017	0.010	0.002	0.198	0.001	0.006	0.215	0.000	0.004	0.002
2018-22, 360	0.078	0.008	0.005	0.001	0.106	0.022	0.005	0.000	0.007	0.005	0.004	0.021	0.012	0.002	0.083	0.000	0.002	0.434	0.000	0.007	0.000
2018-22, 410	0.052	0.003	0.000	0.000	0.040	0.005	0.002	0.000	0.001	0.000	0.000	0.006	0.002	0.000	0.017	0.003	0.001	0.305	2.414	0.000	0.000
2018-22, 460	0.059	0.005	0.002	0.000	0.065	0.006	0.002	0.000	0.001	0.000	0.000	0.007	0.004	0.000	0.044	0.001	0.005	0.230	3.762	0.000	0.000
2018-23, 0	0.181	0.015	0.004	0.000	0.173	0.021	0.003	0.000	0.012	0.009	0.007	0.027	0.020	0.004	0.061	0.001	0.003	0.116	0.021	0.024	0.000
2018-23, 40	0.121	0.011	0.004	0.000	0.125	0.017	0.004	0.000	0.008	0.006	0.006	0.017	0.012	0.003	0.044	0.000	0.002	0.125	0.019	0.013	0.000
2018-23, 100	0.061	0.006	0.002	0.000	0.080	0.013	0.003	0.000	0.009	0.007	0.005	0.020	0.009	0.000	0.020	0.001	0.002	0.123	0.021	0.010	0.000
2018-23, 130	0.101	0.008	0.004	0.001	0.128	0.022	0.007	0.000	0.011	0.007	0.006	0.024	0.014	0.003	0.022	0.001	0.002	0.256	0.000	0.002	0.000
2018-23, 200	0.043	0.007	0.006	0.003	0.050	0.010	0.004	0.000	0.006	0.004	0.002	0.014	0.007	0.001	0.055	0.001	0.001	0.150	0.013	0.006	0.000
2018-23, 220	0.030	0.008	0.007	0.003	0.044	0.009	0.004	0.000	0.005	0.003	0.001	0.013	0.006	0.001	0.061	0.000	0.002	0.161	0.012	0.006	0.000
2018-23, 280	0.051	0.010	0.011	0.003	0.040	0.008	0.004	0.000	0.003	0.001	0.001	0.008	0.004	0.000	0.133	0.000	0.005	0.040	0.009	0.006	0.000
2018-23, 340	0.061	0.012	0.012	0.005	0.074	0.011	0.008	0.000	0.007	0.005	0.002	0.019	0.010	0.000	0.112	0.001	0.003	0.216	0.012	0.006	0.000
2015-16, 620	0.051	0.009	0.004	0.001	0.079	0.015	0.006	0.000	0.009	0.005	0.005	0.022	0.015	0.003	0.103	0.001	0.003	0.255	0.000	0.010	0.000
2016-38, 570	0.047	0.006	0.005	0.002	0.054	0.010	0.003	0.001	0.002	0.001	0.000	0.006	0.003	0.001	0.271	0.000	0.003	0.000	0.000	0.000	0.002
2015-24, 600	0.045	0.016	0.026	0.006	0.048	0.012	0.007	0.000	0.004	0.003	0.002	0.010	0.005	0.001	0.223	0.000	0.003	0.214	0.000	0.004	0.000
2015-29, 500	0.041	0.011	0.010	0.004	0.047	0.014	0.007	0.000	0.006	0.004	0.003	0.016	0.010	0.002	0.095	0.000	0.001	0.180	0.000	0.003	0.000
2018-07, 0	0.133	0.010	0.003	0.000	0.100	0.010	0.000	0.000	0.004	0.005	0.005	0.012	0.011	0.000	0.011	0.002	0.001	0.190	2.221	0.000	0.000
2018-07, 20	0.048	0.009	0.017	0.008	0.039	0.008	0.003	0.000	0.002	0.011	0.000	0.007	0.004	0.000	0.209	0.023	0.037	0.097	1.430	0.000	0.000
2018-07, 40	0.039	0.005	0.006	0.003	0.031	0.012	0.004	0.000	0.015	0.029	0.000	0.017	0.008	0.001	0.851	0.016	0.042	0.051	0.000	0.000	0.000
Average	0.085	0.008	0.005	0.001	0.085	0.017	0.006	0.001	0.006	0.005	0.003	0.016	0.009	0.002	0.185	0.001	0.007	0.131	0.135	0.006	0.000
Maximum	0.250	0.022	0.026	0.008	0.216	0.043	0.016	0.004	0.018	0.029	0.015	0.037	0.027	0.007	1.946	0.023	0.048	0.654	3.762	0.046	0.005
Maximum	0.027	0.002	0.000	0.000	0.023	0.003	0.000	0.000	0.001	0.000	0.000	0.005	0.002	0.000	0.011	0.000	0.000	0.000	0.000	0.000	0.000
Standard deviation	0.050	0.004	0.004	0.001	0.046	0.008	0.003	0.001	0.003	0.004	0.003	0.007	0.005	0.001	0.255	0.003	0.009	0.124	0.592	0.007	0.001

Concentrations are in μg g^{-1} sediment.

Table S6: Concentration of archaeal CLs in Scotian Slope sediments.

	c-GDGTs						OH-GDGTs				GDDs						OH-GDD			BpDiol			
Sample name	GDGT-0	GDGT-1	GDGT-2	GDGT-3	Cren	Cren´	OH-GDGT-0	OH-GDGT-1	OH-GDGT-2	OH-Cren	GDD-0	GDD-1	GDD-2	GDD-3	GDD-4	GDD-Cren	OH-GDD-0	OH-GDD-1	OH-GDD-2	BpDiol-0	BpDiol-1	BpDiol-2	BpDiol-3
2015-1, 180	0.793	0.063	0.031	0.013	0.747	0.005	0.149	0.022	0.006	0.004	0.046	0.005	0.004	0.002	0.039	0.087	0.015	0.003	0.000	0.014	0.003	0.009	0.044
2015-3, 490	0.742	0.044	0.020	0.009	0.841	0.002	0.215	0.026	0.007	0.005	0.081	0.007	0.003	0.000	0.062	0.142	0.035	0.006	0.000	0.034	0.006	0.013	0.068
2015-4, 600	0.944	0.063	0.030	0.012	1.121	0.000	0.246	0.034	0.008	0.007	0.125	0.011	0.006	0.004	0.120	0.266	0.056	0.008	0.000	0.036	0.008	0.020	0.096
2015-6, 220	0.764	0.068	0.039	0.016	0.762	0.008	0.153	0.021	0.006	0.005	0.065	0.008	0.005	0.003	0.051	0.117	0.022	0.004	0.000	0.023	0.003	0.011	0.052
2015-6, 330	0.935	0.086	0.045	0.019	0.954	0.010	0.152	0.025	0.006	0.006	0.066	0.009	0.006	0.004	0.058	0.129	0.018	0.003	0.000	0.021	0.004	0.011	0.054
2015-6, 360	0.585	0.033	0.022	0.013	0.696	0.008	0.163	0.020	0.004	0.004	0.061	0.005	0.003	0.001	0.053	0.121	0.025	0.003	0.000	0.032	0.009	0.015	0.066
2015-6, 500	0.683	0.041	0.033	0.013	0.777	0.005	0.166	0.019	0.004	0.005	0.063	0.006	0.003	0.002	0.054	0.124	0.026	0.002	0.000	0.035	0.005	0.012	0.068
2015-8, 750	0.725	0.039	0.017	0.009	0.707	0.000	0.176	0.018	0.004	0.004	0.046	0.003	0.000	0.000	0.046	0.100	0.017	0.003	0.000	0.016	0.004	0.012	0.046
2016-1, 630	2.144	0.226	0.093	0.032	2.102	0.018	0.770	0.104	0.024	0.015	0.212	0.019	0.011	0.005	0.129	0.296	0.119	0.018	0.005	0.090	0.007	0.049	0.196
2016-3, 160	1.387	0.110	0.046	0.014	1.241	0.007	0.404	0.054	0.010	0.007	0.185	0.014	0.008	0.002	0.110	0.253	0.116	0.015	0.004	0.131	0.007	0.056	0.212
2016-12, 640	1.872	0.123	0.069	0.036	2.059	0.012	0.561	0.074	0.015	0.013	0.307	0.025	0.014	0.008	0.189	0.433	0.143	0.020	0.005	0.193	0.011	0.094	0.326
2016-14, 300	3.365	0.238	0.147	0.070	3.266	0.029	0.899	0.119	0.027	0.021	0.366	0.032	0.021	0.011	0.239	0.540	0.154	0.024	0.004	0.258	0.016	0.134	0.500
2016-14, 380	0.975	0.064	0.037	0.020	1.105	0.008	0.298	0.040	0.008	0.007	0.143	0.012	0.007	0.004	0.095	0.217	0.077	0.010	0.002	0.142	0.005	0.069	0.231
2016-14, 400	1.077	0.081	0.047	0.027	1.102	0.011	0.295	0.043	0.009	0.007	0.166	0.017	0.011	0.007	0.104	0.236	0.078	0.013	0.003	0.138	0.010	0.075	0.259
2016-14, 580	1.179	0.080	0.044	0.026	1.092	0.009	0.370	0.048	0.011	0.008	0.194	0.018	0.011	0.007	0.114	0.261	0.093	0.013	0.004	0.130	0.008	0.071	0.246
2016-14, 780	2.026	0.193	0.090	0.039	2.026	0.008	0.606	0.083	0.018	0.013	0.258	0.022	0.012	0.006	0.173	0.399	0.119	0.018	0.005	0.106	0.004	0.045	0.184
2016-14, 870	3.325	0.259	0.129	0.059	3.683	0.021	0.890	0.120	0.028	0.021	0.411	0.035	0.017	0.011	0.302	0.709	0.202	0.030	0.007	0.269	0.013	0.119	0.444
2015-9, 150	1.420	0.098	0.035	0.013	1.343	0.008	0.291	0.032	0.005	0.008	0.073	0.007	0.003	0.000	0.068	0.151	0.019	0.003	0.000	0.021	0.003	0.009	0.055
2015-9, 300	1.004	0.082	0.030	0.009	0.996	0.000	0.203	0.034	0.007	0.006	0.071	0.007	0.004	0.000	0.057	0.126	0.023	0.004	0.000	0.016	0.003	0.007	0.036
2015-9, 370	1.284	0.106	0.037	0.011	1.257	0.008	0.284	0.040	0.008	0.009	0.093	0.009	0.004	0.000	0.071	0.159	0.036	0.005	0.000	0.020	0.003	0.003	0.047
2015-11, 350	1.471	0.143	0.052	0.009	1.020	0.006	0.377	0.059	0.013	0.010	0.116	0.011	0.007	0.001	0.053	0.125	0.050	0.011	0.000	0.021	0.000	0.014	0.054
2015-12, 700	1.759	0.203	0.062	0.016	1.554	0.009	0.353	0.045	0.015	0.008	0.131	0.014	0.008	0.002	0.095	0.209	0.033	0.006	0.000	0.062	0.015	0.032	0.131
2015-13, 700	1.441	0.160	0.051	0.011	1.387	0.011	0.246	0.035	0.010	0.009	0.110	0.013	0.006	0.002	0.082	0.180	0.023	0.004	0.000	0.030	0.005	0.015	0.069
2016-15, 690	1.731	0.141	0.062	0.030	1.578	0.012	0.490	0.060	0.013	0.009	0.205	0.019	0.011	0.006	0.138	0.316	0.111	0.016	0.004	0.155	0.009	0.085	0.321
2016-17, 470	2.784	0.242	0.125	0.032	2.691	0.021	0.660	0.088	0.019	0.017	0.289	0.026	0.014	0.005	0.177	0.415	0.103	0.018	0.005	0.161	0.015	0.098	0.380
2016-20, 720	1.726	0.241	0.118	0.024	1.811	0.023	0.343	0.062	0.017	0.010	0.157	0.020	0.011	0.002	0.098	0.225	0.059	0.010	0.003	0.076	0.008	0.038	0.170
2016-22, 600	4.566	0.878	0.414	0.065	4.094	0.072	0.940	0.209	0.066	0.043	0.401	0.051	0.027	0.006	0.234	0.535	0.110	0.018	0.008	0.090	0.010	0.050	0.204
2016-24, 700	3.809	0.503	0.172	0.042	3.750	0.046	0.939	0.164	0.040	0.052	0.452	0.048	0.022	0.005	0.247	0.565	0.127	0.026	0.007	0.165	0.012	0.071	0.287
2016-25, 270	1.594	0.143	0.081	0.038	1.648	0.015	0.381	0.053	0.014	0.008	0.156	0.018	0.013	0.007	0.102	0.233	0.059	0.011	0.003	0.101	0.011	0.060	0.235
2016-25, 290	4.044	0.324	0.191	0.095	3.722	0.025	0.859	0.104	0.033	0.018	0.374	0.042	0.029	0.014	0.239	0.536	0.128	0.017	0.006	0.229	0.021	0.142	0.506
2016-25, 300	1.583	0.148	0.101	0.058	1.670	0.014	0.334	0.053	0.015	0.009	0.192	0.023	0.016	0.010	0.117	0.271	0.069	0.012	0.003	0.130	0.011	0.070	0.230
2016-25, 800	1.879	0.208	0.088	0.025	1.839	0.017	0.546	0.071	0.015	0.010	0.136	0.013	0.007	0.002	0.090	0.210	0.064	0.010	0.003	0.066	0.006	0.042	0.154
2016-26, 490	2.390	0.284	0.103	0.035	2.004	0.015	0.877	0.135	0.028	0.016	0.200	0.018	0.010	0.004	0.126	0.294	0.100	0.016	0.005	0.051	0.004	0.032	0.133
2016-28, 660	1.955	0.170	0.080	0.030	1.750	0.014	0.694	0.080	0.016	0.009	0.173	0.016	0.009	0.004	0.104	0.237	0.099	0.013	0.003	0.113	0.008	0.054	0.164
2016-29, 700	2.067	0.219	0.120	0.049	2.087	0.025	0.590	0.083	0.019	0.017	0.231	0.027	0.017	0.007	0.148	0.349	0.102	0.017	0.005	0.085	0.005	0.041	0.130
2016-30, 630	2.484	0.129	0.058	0.028	2.246	0.010	0.917	0.065	0.009	0.011	0.239	0.015	0.008	0.005	0.179	0.410	0.166	0.017	0.003	0.189	0.011	0.083	0.348
2016-49, 450	1.894	0.276	0.139	0.058	1.727	0.013	0.396	0.058	0.014	0.009	0.205	0.028	0.019	0.010	0.132	0.297	0.083	0.013	0.005	0.122	0.010	0.075	0.229
2018-21, 0	2.897	0.367	0.183	0.034	2.711	0.029	0.398	0.073	0.024	0.018	0.041	0.005	0.000	0.000	0.035	0.078	0.014	0.002	0.000	0.008	0.000	0.000	0.027
2018-21, 60	4.255	0.588	0.232	0.043	3.437	0.037	0.682	0.128	0.037	0.032	0.012	0.000	0.000	0.000	0.008	0.019	0.004	0.000	0.000	0.000	0.000	0.000	0.000
2018-21, 140	1.995	0.219	0.112	0.019	1.601	0.018	0.359	0.060	0.018	0.015	0.014	0.000	0.000	0.000	0.012	0.023	0.006	0.001	0.000	0.000	0.000	0.000	0.000
2018-21, 210	2.093	0.142	0.055	0.021	1.962	0.007	0.390	0.055	0.012	0.011	0.092	0.009	0.005	0.002	0.077	0.177	0.036	0.006	0.000	0.018	0.000	0.005	0.043
2018-21, 240	1.454	0.121	0.048	0.017	1.176	0.007	0.265	0.036	0.010	0.011	0.021	0.000	0.000	0.000	0.013	0.035	0.006	0.000	0.000	0.000	0.000	0.000	0.000
2018-21, 320	1.278	0.128	0.047	0.013	1.094	0.006	0.227	0.030	0.011	0.006	0.086	0.009	0.004	0.000	0.057	0.123	0.025	0.004	0.000	0.029	0.000	0.014	0.072
2018-21, 410	1.235	0.092	0.030	0.011	1.091	0.005	0.257	0.034	0.007	0.010	0.041	0.003	0.000	0.000	0.028	0.062	0.013	0.001	0.000	0.014	0.000	0.000	0.032
2018-21, 450	0.723	0.047	0.016	0.006	0.615	0.000	0.197	0.021	0.004	0.004	0.032	0.000	0.000	0.000	0.024	0.053	0.012	0.002	0.000	0.022	0.000	0.009	0.050
2018-21, 520	3.228	0.290	0.102	0.030	3.093	0.014	0.483	0.074	0.019	0.022	0.106	0.008	0.000	0.000	0.085	0.183	0.024	0.006	0.000	0.024	0.000	0.006	0.051
2018-21, 570	1.307	0.071	0.032	0.012	1.221	0.000	0.253	0.028	0.006	0.008	0.116	0.009	0.007	0.000	0.098	0.212	0.034	0.007	0.000	0.034	0.003	0.015	0.069
2018-21, 610	1.525	0.151	0.051	0.014	1.384	0.008	0.222	0.031	0.008	0.006	0.081	0.008	0.004	0.002	0.063	0.137	0.017	0.003	0.000	0.032	0.005	0.015	0.068
2018-21, 670	0.370	0.032	0.011	0.004	0.321	0.002	0.079	0.008	0.002	0.001	0.014	0.000	0.000	0.000	0.011	0.027	0.005	0.000	0.000	0.013	0.002	0.006	0.026
2018-21, 710	1.326	0.136	0.044	0.012	1.184	0.010	0.215	0.025	0.008	0.005	0.041	0.004	0.000	0.000	0.031	0.068	0.009	0.001	0.000	0.021	0.002	0.008	0.042
2018-22, 0	4.845	0.785	0.326	0.060	4.320	0.075	0.544	0.127	0.042	0.031	0.073	0.010	0.008	0.000	0.064	0.146	0.018	0.003	0.000	0.016	0.000	0.000	0.045
2018-22, 60	5.909	0.963	0.397	0.079	4.675	0.064	0.725	0.134	0.039	0.034	0.084	0.011	0.007	0.000	0.067	0.150	0.024	0.005	0.000	0.010	0.000	0.000	0.027
2018-22, 110	2.615	0.249	0.091	0.033	2.322	0.013	0.426	0.069	0.015	0.015	0.057	0.006	0.000	0.000	0.050	0.107	0.018	0.003	0.000	0.008	0.000	0.000	0.018
2018-22, 150	1.433	0.148	0.065	0.032	1.599	0.008	0.234	0.035	0.009	0.009	0.134	0.019	0.010	0.007	0.111	0.248	0.036	0.006	0.000	0.029	0.000	0.012	0.065
2018-22, 270	1.573	0.133	0.053	0.021	1.570	0.000	0.263	0.035	0.009	0.007	0.105	0.011	0.007	0.004	0.089	0.195	0.029	0.006	0.000	0.029	0.000	0.016	0.070
2018-22, 300	2.067	0.230	0.093	0.041	1.899	0.000	0.334	0.042	0.013	0.010	0.049	0.006	0.003	0.000	0.039	0.084	0.014	0.001	0.000	0.015	0.000	0.008	0.032
2018-22, 360	1.896	0.190	0.072	0.027	1.863	0.014	0.274	0.044	0.012	0.012	0.131	0.015	0.009	0.003	0.111	0.246	0.036	0.006	0.000	0.027	0.000	0.013	0.074
2018-22, 410	1.411	0.131	0.045	0.011	1.244	0.006	0.209	0.029	0.009	0.006	0.060	0.006	0.000	0.000	0.046	0.105	0.009	0.002	0.000	0.014	0.000	0.013	0.054
2018-22, 460	0.697	0.051	0.020	0.007	0.691	0.000	0.132	0.015	0.002	0.004	0.067	0.006	0.000	0.000	0.064	0.151	0.017	0.002	0.000	0.036	0.000	0.022	0.117
2018-23, 0	3.764	0.527	0.216	0.040	3.624	0.034	0.374	0.067	0.020	0.016	0.084	0.011	0.007	0.000	0.096	0.210	0.018	0.001	0.000	0.022	0.000	0.000	0.071
2018-23, 40	3.230	0.546	0.250	0.038	3.075	0.044	0.266	0.058	0.019	0.015	0.099	0.016	0.012	0.000	0.107	0.236	0.019	0.004	0.000	0.018	0.000	0.004	0.050
2018-23, 100	2.493	0.316	0.127	0.029	2.274	0.015	0.364	0.045	0.012	0.011	0.078	0.011	0.008	0.000	0.064	0.150	0.016	0.002	0.000	0.011	0.000	0.008	0.032
2018-23, 130	2.544	0.292	0.112	0.027	2.328	0.020	0.360	0.055	0.015	0.014	0.079	0.010	0.007	0.000	0.075	0.170	0.020	0.003	0.000	0.011	0.000	0.000	0.030
2018-23, 200	1.789	0.192	0.082	0.039	1.725	0.000	0.224	0.030	0.010	0.005	0.067	0.009	0.006	0.000	0.074	0.161	0.015	0.003	0.000	0.020	0.000	0.010	0.052
2018-23, 220	1.986	0.201	0.094	0.055	1.936	0.009	0.268	0.045	0.010	0.007	0.100	0.016	0.011	0.000	0.111	0.249	0.023	0.004	0.000	0.026	0.000	0.014	0.085
2018-23, 280	0.931	0.133	0.069	0.045	0.951	0.008	0.114	0.021	0.010	0.005	0.069	0.010	0.009	0.000	0.061	0.130	0.014	0.003	0.000	0.024	0.000	0.013	0.049
2018-23, 340	2.048	0.218	0.097	0.062	2.059	0.000	0.279	0.039	0.014	0.009	0.095	0.013	0.012	0.000	0.095	0.203	0.020	0.004	0.000	0.027	0.000	0.000	0.066
2015-16, 620	1.709	0.176	0.057	0.022	1.480	0.011	0.295	0.041	0.010	0.009	0.130	0.013	0.008	0.003	0.097	0.219	0.029	0.006	0.000	0.036	0.010	0.017	0.082
2016-38, 570	1.347	0.133	0.076	0.037	1.312	0.011	0.394	0.050	0.012	0.008	0.169	0.019	0.013	0.007	0.111	0.260	0.082	0.012	0.004	0.092	0.007	0.047	0.167
2015-24, 600	1.495	0.307	0.168	0.095	1.511	0.023	0.220	0.044	0.018	0.008	0.138	0.028	0.025	0.017	0.121	0.239	0.033	0.008	0.000	0.041	0.009	0.026	0.083
2015-29, 500	1.871	0.222	0.100	0.053	1.665	0.011	0.262	0.044	0.011	0.008	0.099	0.015	0.012	0.007	0.079	0.174	0.024	0.005	0.000	0.028	0.005	0.011	0.070
2018-07, 0	2.700	0.509	0.243	0.051	2.883	0.043	0.200	0.056	0.016	0.020	0.093	0.018	0.012	0.000	0.109	0.226	0.007	0.000	0.000	0.017	0.000	0.011	0.082
2018-07, 20	1.128	0.261	0.510	0.400	0.931	0.000	0.141	0.045	0.025	0.006	0.060	0.013	0.014	0.008	0.052	0.120	0.012	0.003	0.000	0.019	0.000	0.095	0.042
2018-07, 40	1.475	1.239	3.461	2.233	0.791	0.000	0.208	0.372	0.219	0.005	0.100	0.013	0.012	0.006	0.060	0.132	0.029	0.008	0.004	0.036	0.000	0.057	0.058
Average	1.933	0.230	0.147	0.066	1.812	0.014	0.383	0.061	0.018	0.012	0.131	0.014	0.008	0.003	0.094	0.213	0.049	0.008	0.001	0.059	0.005	0.031	0.121
Maximum	5.909	1.239	3.461	2.233	4.675	0.075	0.940	0.372	0.219	0.052	0.452	0.051	0.029	0.017	0.302	0.709	0.202	0.030	0.008	0.269	0.021	0.142	0.506
Minimum	0.370	0.032	0.011	0.004	0.321	0.000	0.079	0.008	0.002	0.001	0.012	0.000	0.000	0.000	0.008	0.019	0.004	0.000	0.000	0.000	0.000	0.000	0.000
Standard deviation	1.084	0.219	0.402	0.260	0.970	0.016	0.227	0.052	0.026	0.009	0.098	0.010	0.007	0.004	0.059	0.135	0.046	0.007	0.002	0.064	0.005	0.035	0.117

Concentrations are in μg g^{-1} sediment.

Table S7: Archaeal lipid diagenetic alteration ratios.

Sample name	1G-GDGTs/(1G-GDGTs+GDGTs+GDDs)	1G-GDGT-5/(1G-Cren+Cren+GDD-5)	2G-GDGTs/(2G-GDGTs+GDGTs+GDDs)	2G-AR/(AR+2G-AR)	1G-OH-GDGTs/(1G-OH-GDGTs+OH-GDGTs+OH-GDDs)	2G-OH-GDGTs/(2G-OH-GDGTs+OH-GDGTs+OH-GDDs)	PA-AR/(PA-AR+AR)	1G-AR/(AR+1G-AR)	GDGTs/(GDGTs+GDDs)	OH-GDGTs/(OH-GDGTs+OH-GDDs)	Cren/(Cren+GDD-5)	GDDs/(GDDs+BpDiols)
2018-07, 0	0.03	0.03	0.00	0.11	0.03	0.07	0.95	0.17	0.93	0.98	0.93	0.81
2018-21, 0	0.05	0.05	0.00	0.04	0.04	0.08	0.62	0.00	0.97	0.97	0.97	0.82
2018-22, 0	0.04	0.05	0.00	0.02	0.04	0.07	0.64	0.01	0.97	0.97	0.97	0.83
2018-23, 0	0.04	0.04	0.00	0.04	0.05	0.09	0.66	0.01	0.95	0.96	0.95	0.81
2018-07, 20	0.03	0.04	0.00	0.15	0.04	0.04	0.32	0.10	0.92	0.94	0.89	0.63
2018-23, 40	0.03	0.04	0.00	0.05	0.05	0.08	0.74	0.01	0.94	0.94	0.93	0.87
2018-07, 40	0.01	0.03	0.00	0.05	0.02	0.03	0.06	0.02	0.97	0.96	0.86	0.68
2018-21, 60	0.05	0.06	0.01	0.14	0.05	0.07	0.75	0.00	1.00	1.00	0.99	1.00
2018-22, 60	0.02	0.03	0.00	0.06	0.04	0.05	0.80	0.01	0.97	0.97	0.97	0.89
2018-23, 100	0.03	0.03	0.00	0.07	0.03	0.06	0.86	0.02	0.94	0.96	0.94	0.86
2018-22, 110	0.03	0.03	0.00	0.05	0.04	0.06	0.87	0.00	0.96	0.96	0.96	0.89
2018-23, 130	0.04	0.05	0.00	0.07	0.06	0.08	0.92	0.02	0.94	0.95	0.93	0.89
2018-21, 140	0.05	0.05	0.01	0.06	0.06	0.08	0.84	0.00	0.99	0.98	0.99	1.00
2018-22, 150	0.04	0.04	0.00	0.04	0.06	0.04	0.61	0.00	0.86	0.87	0.87	0.83
2015-9, 150	0.03	0.03	0.00	0.08	0.04	0.04	0.88	0.04	0.91	0.94	0.90	0.77
2016-3, 160	0.04	0.04	0.00	0.00	0.04	0.04	0.00	0.00	0.83	0.78	0.83	0.58
2015-1, 180	0.03	0.03	0.01	0.06	0.04	0.08	0.80	0.01	0.90	0.91	0.90	0.72
2018-23, 200	0.03	0.03	0.00	0.02	0.05	0.07	0.73	0.01	0.92	0.94	0.91	0.80
2018-21, 210	0.02	0.03	0.00	0.05	0.04	0.04	0.79	0.03	0.92	0.92	0.92	0.85
2018-23, 220	0.02	0.02	0.00	0.03	0.03	0.05	0.72	0.00	0.90	0.93	0.89	0.80
2015-6, 220	0.04	0.04	0.01	0.05	0.05	0.08	0.56	0.00	0.87	0.88	0.87	0.74
2018-21, 240	0.06	0.07	0.00	0.06	0.06	0.08	0.77	0.01	0.98	0.98	0.97	1.00
2018-22, 270	0.04	0.04	0.00	0.03	0.06	0.07	0.70	0.01	0.89	0.90	0.89	0.78
2016-25, 270	0.04	0.03	0.00	0.02	0.06	0.04	0.00	0.00	0.87	0.86	0.88	0.57
2018-23, 280	0.05	0.04	0.00	0.03	0.07	0.07	0.23	0.00	0.88	0.90	0.88	0.76
2016-25, 290	0.04	0.03	0.00	0.02	0.04	0.03	0.05	0.01	0.87	0.87	0.87	0.58
2016-14, 300	0.06	0.05	0.00	0.10	0.04	0.03	0.00	0.00	0.85	0.85	0.86	0.57
2015-9, 300	0.04	0.04	0.01	0.28	0.07	0.07	0.83	0.00	0.89	0.90	0.89	0.81
2016-25, 300	0.04	0.03	0.00	0.03	0.05	0.06	0.00	0.00	0.85	0.83	0.86	0.59
2018-22, 300	0.05	0.06	0.00	0.03	0.06	0.07	0.52	0.00	0.96	0.96	0.96	0.77
2018-21, 320	0.02	0.03	0.00	0.05	0.04	0.07	0.80	0.02	0.90	0.90	0.90	0.71
2015-6, 330	0.03	0.03	0.00	0.00	0.04	0.10	0.85	0.00	0.88	0.90	0.88	0.75
2018-23, 340	0.03	0.03	0.00	0.03	0.05	0.07	0.66	0.01	0.91	0.93	0.91	0.82

2015-11, 350	0.04	0.05	0.01	0.03	0.11	0.08	0.41	0.00	0.90	0.88	0.89	0.78
2015-6, 360	0.07	0.06	0.00	0.07	0.06	0.08	0.24	0.00	0.85	0.87	0.85	0.67
2018-22, 360	0.04	0.05	0.00	0.02	0.07	0.08	0.84	0.00	0.89	0.89	0.88	0.82
2015-9, 370	0.03	0.04	0.00	0.07	0.05	0.06	0.80	0.01	0.89	0.89	0.89	0.82
2016-14, 380	0.06	0.05	0.00	0.04	0.06	0.04	0.00	0.00	0.82	0.80	0.84	0.52
2016-14, 400	0.05	0.04	0.00	0.03	0.05	0.03	0.00	0.00	0.81	0.79	0.82	0.53
2018-22, 410	0.03	0.03	0.00	0.07	0.03	0.03	0.95	0.13	0.93	0.96	0.92	0.73
2018-21, 410	0.08	0.08	0.01	0.03	0.08	0.10	0.76	0.01	0.95	0.95	0.95	0.74
2018-21, 450	0.09	0.10	0.00	0.06	0.06	0.07	0.70	0.01	0.93	0.94	0.92	0.57
2016-49, 450	0.02	0.02	0.00	0.00	0.03	0.01	0.00	0.00	0.86	0.82	0.85	0.61
2018-22, 460	0.07	0.07	0.00	0.11	0.05	0.06	0.84	0.02	0.84	0.89	0.82	0.62
2016-17, 470	0.04	0.04	0.00	0.01	0.05	0.03	0.00	0.01	0.86	0.86	0.87	0.59
2015-3, 490	0.05	0.05	0.01	0.08	0.06	0.07	0.47	0.01	0.85	0.86	0.86	0.71
2016-26, 490	0.03	0.03	0.00	0.01	0.03	0.03	0.00	0.00	0.88	0.90	0.87	0.75
2015-29, 500	0.03	0.02	0.00	0.02	0.05	0.07	0.66	0.00	0.91	0.92	0.91	0.77
2015-6, 500	0.06	0.04	0.00	0.07	0.07	0.07	0.33	0.02	0.86	0.87	0.86	0.68
2018-21, 520	0.04	0.04	0.00	0.04	0.06	0.08	0.87	0.02	0.95	0.95	0.94	0.83
2018-21, 570	0.07	0.08	0.00	0.03	0.09	0.08	0.83	0.00	0.86	0.88	0.85	0.79
2016-38, 570	0.03	0.03	0.00	0.01	0.02	0.02	0.00	0.00	0.83	0.83	0.83	0.65
2016-14, 580	0.06	0.05	0.00	0.03	0.04	0.04	0.00	0.00	0.80	0.80	0.81	0.57
2015-24, 600	0.03	0.03	0.00	0.01	0.05	0.05	0.49	0.00	0.86	0.87	0.86	0.78
2015-4, 600	0.05	0.04	0.00	0.06	0.07	0.07	0.46	0.02	0.80	0.82	0.81	0.77
2016-22, 600	0.02	0.02	0.00	0.01	0.02	0.02	0.00	0.00	0.89	0.90	0.88	0.78
2018-21, 610	0.04	0.05	0.00	0.03	0.04	0.07	0.76	0.04	0.91	0.93	0.91	0.71
2015-16, 620	0.04	0.04	0.00	0.03	0.05	0.09	0.71	0.01	0.88	0.91	0.87	0.76
2016-12, 640	0.05	0.05	0.00	0.00	0.04	0.02	0.00	0.00	0.81	0.80	0.83	0.61
2016-1, 630	0.04	0.04	0.00	0.07	0.03	0.02	0.00	0.00	0.87	0.87	0.88	0.66
2016-30, 630	0.06	0.07	0.00	0.02	0.03	0.05	0.00	0.00	0.85	0.84	0.85	0.58
2016-28, 660	0.03	0.03	0.00	0.01	0.02	0.02	0.00	0.00	0.88	0.87	0.88	0.62
2018-21, 670	0.07	0.08	0.00	0.08	0.04	0.07	0.44	0.03	0.93	0.95	0.92	0.53
2016-15, 690	0.05	0.04	0.00	0.05	0.04	0.02	0.00	0.01	0.84	0.81	0.83	0.55
2015-12, 700	0.05	0.06	0.00	0.06	0.04	0.07	0.74	0.01	0.89	0.92	0.88	0.66
2015-13, 700	0.04	0.05	0.00	0.04	0.06	0.09	0.78	0.01	0.89	0.92	0.89	0.77
2016-24, 700	0.03	0.03	0.00	0.01	0.02	0.03	0.00	0.00	0.86	0.88	0.87	0.71
2016-29, 700	0.03	0.04	0.00	0.01	0.03	0.02	0.00	0.00	0.85	0.85	0.86	0.75
2018-21, 710	0.05	0.06	0.00	0.03	0.05	0.08	0.69	0.01	0.95	0.96	0.95	0.66
2016-20, 720	0.03	0.02	0.00	0.02	0.04	0.05	0.00	0.00	0.88	0.86	0.89	0.64
2015-8, 750	0.08	0.07	0.00	0.11	0.09	0.09	0.76	0.04	0.88	0.91	0.88	0.72
2016-14, 780	0.03	0.03	0.00	0.03	0.04	0.02	0.00	0.00	0.83	0.84	0.84	0.72
2016-25, 800	0.04	0.04	0.00	0.02	0.04	0.05	0.00	0.00	0.90	0.89	0.90	0.63
2016-14, 870	0.03	0.03	0.00	0.03	0.03	0.02	0.00	0.00	0.83	0.82	0.84	0.64

Table S8: Mean relative abundance of slope archaeal lipid associated with diagenetic alteration.

Depth interval (mbsf)	[1G-GDGTs/(1G-GDGTs+GDGTs+GDDs)]*100	[1G-Cren/(1G-Cren+Cren+GDD-5)]*100	[1G-OH-GDGTs/(1G-OH-GDGTs+OH-GDGTs+OH-GDDs)]*100	[2G-GDGTs/(2G-GDGTs+GDGTs+GDDs)]*100	[2G-OH-GDGTs/(2G-OH-GDGTs+OH-GDGTs+OH-GDDs)]*100	[GDGTs/(GDGTs+GDDs)]*100	[OH-GDGTs/(OH-GDGTs+OH-GDDs)]*100	[Cren/(Cren+GDD-5)]*100	[GDDs/(GDDs+BpDiols)]*100	[PA-AR/(PA-AR+AR)]*100	[1G-AR/(AR+1G-AR)]*100	[2G-AR/(AR+2G-AR)]*100
0-1	3.4	4.0	4.0	0.4	6.5	95.8	96.4	93.9	82.0	63.8	3.5	7.3
1-2	3.4	3.7	4.9	0.4	6.1	91.4	91.6	91.0	81.3	70.8	1.1	4.8
2-3	4.1	4.0	5.3	0.3	5.7	89.4	89.8	89.4	73.4	43.1	0.6	6.1
3-4	4.3	4.2	5.9	0.4	6.9	87.2	87.4	87.4	71.1	51.0	0.4	3.7
4-5	5.0	5.0	5.2	0.3	5.6	88.6	89.8	88.2	67.7	47.0	2.2	4.6
5-6	4.2	4.2	5.0	0.2	5.1	85.6	86.5	85.6	73.7	37.7	0.7	2.6
6-7	4.4	4.8	3.7	0.2	4.7	87.2	87.9	87.2	65.8	28.7	1.0	3.2
7-8	4.4	4.4	5.3	0.2	5.6	89.0	89.2	88.9	67.3	28.9	1.1	4.3
8-9	2.9	2.6	3.5	0.1	1.9	83.4	81.6	83.9	63.7	0.0	0.2	2.6
% transformation over full depth interval	0.5	1.4	0.5	0.3	4.5	12.4	14.8	10.0	18.3	63.8	3.4	4.7
% transformation per m	0.1	0.2	0.1	0.03	0.5	1.4	1.6	1.1	2.0	7.1	0.4	0.5

Table S9: Archaeal lipid sourcing ratios.

Sample name	MI	GDGT-0 /Cren	GDGT-2 /Cren	1G-MI	1G-GDGT-0 /1G-Cren	1G-GDGT-2 /1G-Cren	Hydrocarbon detection
2015-1, 180	0.13	1.06	0.04	0.24	1.17	0.12	Ambient
2015-3, 490	0.08	0.88	0.02	0.14	1.07	0.06	Ambient
2015-4, 600	0.09	0.84	0.03	0.16	1.05	0.07	Ambient
2015-6, 220	0.14	1.00	0.05	0.28	1.02	0.21	
2015-6, 330	0.13	0.98	0.05	0.23	1.19	0.16	
2015-6, 360	0.09	0.84	0.03	0.12	1.13	0.03	
2015-6, 500	0.10	0.88	0.04	0.19	1.33	0.10	Ambient
2015-8, 750	0.08	1.03	0.02	0.10	1.23	0.02	Ambient
2016-1, 630	0.14	1.02	0.04	0.13	1.21	0.04	Ambient
2016-3, 160	0.12	1.12	0.04	0.15	1.16	0.05	Ambient
2016-12, 640	0.10	0.91	0.03	0.13	1.20	0.05	Ambient
2016-14, 300	0.12	1.03	0.05	0.14	1.16	0.06	
2016-14, 380	0.10	0.88	0.03	0.13	1.31	0.05	
2016-14, 400	0.12	0.98	0.04	0.17	1.36	0.09	
2016-14, 580	0.12	1.08	0.04	0.16	1.25	0.08	
2016-14, 780	0.14	1.00	0.04	0.16	0.88	0.07	
2016-14, 870	0.11	0.90	0.04	0.15	1.09	0.06	Ambient
2015-9, 150	0.10	1.06	0.03	0.09	0.82	0.02	
2015-9, 300	0.11	1.01	0.03	0.10	0.99	0.03	
2015-9, 370	0.11	1.02	0.03	0.12	0.79	0.04	Ambient
2015-11, 350	0.17	1.44	0.05	0.15	0.90	0.06	Ambient
2015-12, 700	0.15	1.13	0.04	0.10	0.65	0.02	Ambient
2015-13, 700	0.14	1.04	0.04	0.10	0.82	0.02	Ambient
2016-15, 690	0.13	1.10	0.04	0.15	1.43	0.07	Ambient
2016-17, 470	0.13	1.03	0.05	0.12	1.23	0.04	Ambient
2016-20, 720	0.17	0.95	0.07	0.14	1.64	0.05	Ambient
2016-22, 600	0.25	1.12	0.10	0.10	1.02	0.03	Ambient
2016-24, 700	0.16	1.02	0.05	0.09	1.35	0.02	Ambient
2016-25, 270	0.14	0.97	0.05	0.23	1.54	0.13	
2016-25, 290	0.14	1.09	0.05	0.20	1.40	0.09	
2016-25, 300	0.15	0.95	0.06	0.25	1.40	0.14	
2016-25, 800	0.15	1.02	0.05	0.13	1.04	0.04	Ambient
2016-26, 490	0.17	1.19	0.05	0.14	0.73	0.05	Ambient
2016-28, 660	0.14	1.12	0.05	0.14	0.80	0.07	Ambient
2016-29, 700	0.16	0.99	0.06	0.16	0.94	0.07	Ambient
2016-30, 630	0.09	1.11	0.03	0.07	0.86	0.02	Ambient
2016-49, 450	0.21	1.10	0.08	0.25	1.20	0.17	Ambient
2018-21, 0	0.18	1.07	0.07	0.11	1.15	0.03	
2018-21, 60	0.20	1.24	0.07	0.13	1.12	0.04	
2018-21, 140	0.18	1.25	0.07	0.12	1.07	0.04	
2018-21, 210	0.10	1.07	0.03	0.11	0.55	0.03	
2018-21, 240	0.14	1.24	0.04	0.13	1.02	0.05	
2018-21, 320	0.15	1.17	0.04	0.14	0.90	0.05	
2018-21, 410	0.11	1.13	0.03	0.10	1.08	0.03	
2018-21, 450	0.10	1.18	0.03	0.10	1.01	0.03	Ambient

2018-21, 520	0.12	1.04	0.03	0.12	0.88	0.03	
2018-21, 570	0.09	1.07	0.03	0.09	0.80	0.02	
2018-21, 610	0.13	1.10	0.04	0.10	0.73	0.03	
2018-21, 670	0.13	1.15	0.03	0.10	0.90	0.03	
2018-21, 710	0.14	1.12	0.04	0.09	0.83	0.02	
2018-22, 0	0.21	1.12	0.08	0.11	0.96	0.03	
2018-22, 60	0.23	1.26	0.08	0.11	0.59	0.04	
2018-22, 110	0.14	1.13	0.04	0.12	0.61	0.05	
2018-22, 150	0.13	0.90	0.04	0.21	0.79	0.12	
2018-22, 270	0.12	1.00	0.03	0.12	0.82	0.03	
2018-22, 300	0.16	1.09	0.05	0.16	0.76	0.08	
2018-22, 360	0.13	1.02	0.04	0.12	0.74	0.04	
2018-22, 410	0.13	1.13	0.04	0.08	1.28	0.01	
2018-22, 460	0.10	1.01	0.03	0.10	0.90	0.03	Ambient
2018-23, 0	0.18	1.04	0.06	0.10	1.05	0.02	
2018-23, 40	0.21	1.05	0.08	0.11	0.97	0.03	
2018-23, 100	0.17	1.10	0.06	0.09	0.77	0.03	
2018-23, 130	0.16	1.09	0.05	0.09	0.79	0.03	
2018-23, 200	0.15	1.04	0.05	0.24	0.86	0.11	
2018-23, 220	0.15	1.03	0.05	0.29	0.69	0.17	
2018-23, 280	0.20	0.98	0.07	0.37	1.27	0.27	
2018-23, 340	0.15	0.99	0.05	0.27	0.82	0.16	Ambient
2015-16, 620	0.15	1.15	0.04	0.14	0.65	0.04	Ambient
2016-38, 570	0.16	1.03	0.06	0.20	0.88	0.10	Ambient
2015-24, 600	0.27	0.99	0.11	0.50	0.95	0.55	Ambient
2015-29, 500	0.18	1.12	0.06	0.34	0.87	0.22	Ambient
Average	0.14	1.06	0.05	0.15	1.01	0.07	
Maximum	0.27	1.44	0.11	0.50	1.64	0.55	
Minimum	0.08	0.84	0.02	0.07	0.55	0.01	
Standard deviation	0.04	0.10	0.02	0.08	0.24	0.08	
2018-07, 0	0.22	0.94	0.08	0.12	1.33	0.03	Seep
2018-07, 20	0.56	1.21	0.55	0.47	1.24	0.43	
2018-07, 40	0.90	1.86	4.37	0.32	1.27	0.20	
Average	0.56	1.34	1.67	0.30	1.28	0.22	
Maximum	0.90	1.86	4.37	0.47	1.33	0.43	
Minimum	0.22	0.94	0.08	0.12	1.24	0.03	
Standard deviation	0.34	0.48	2.35	0.18	0.05	0.20	

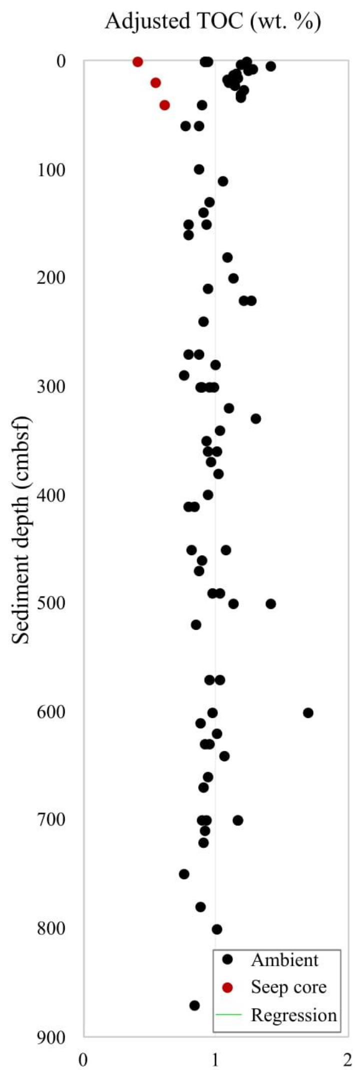

Figure S1: Down core $TOC_{adjusted}$ trend of the Scotian Slope sediment samples.

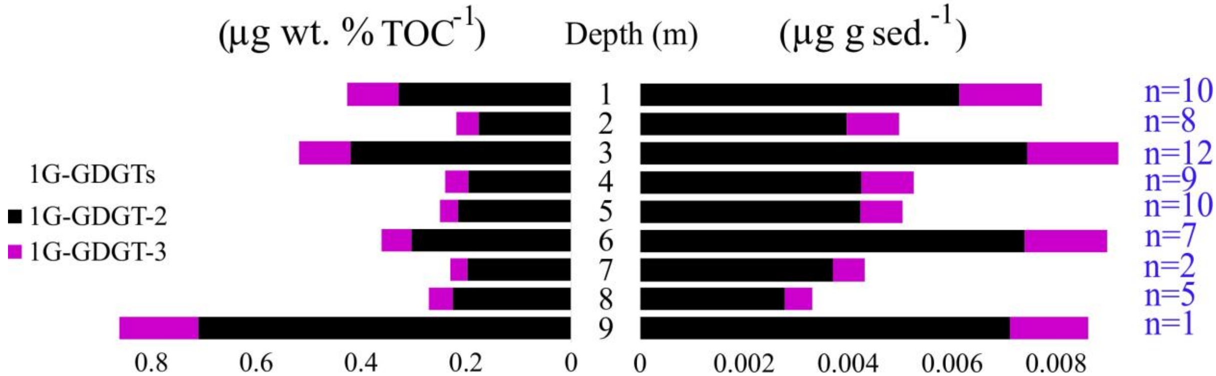

Figure S2: Bar graphs of down-core 1G-GDGT-2 and -3 abundances normalized to sediment (right) and TOC (left) (blue font "n" indicates the summed samples for each depth interval).

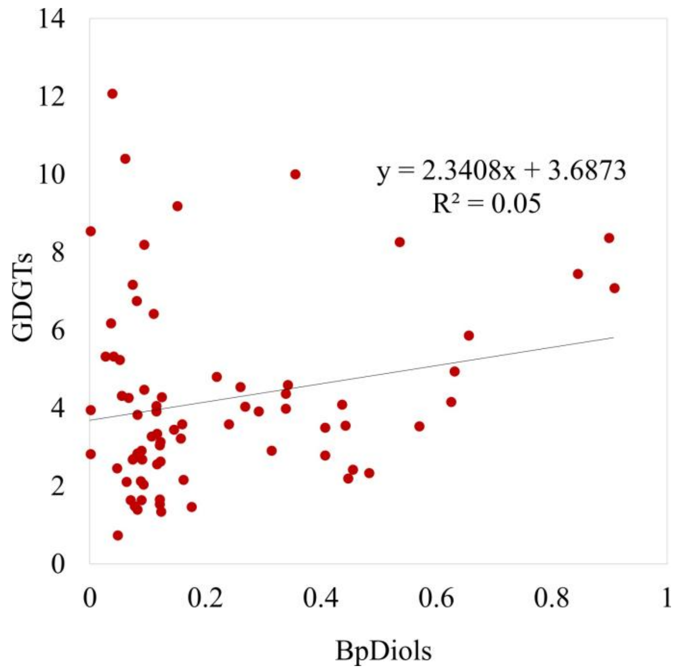

Figure S3: Cross plot of GDGT and BpDiol concentrations.

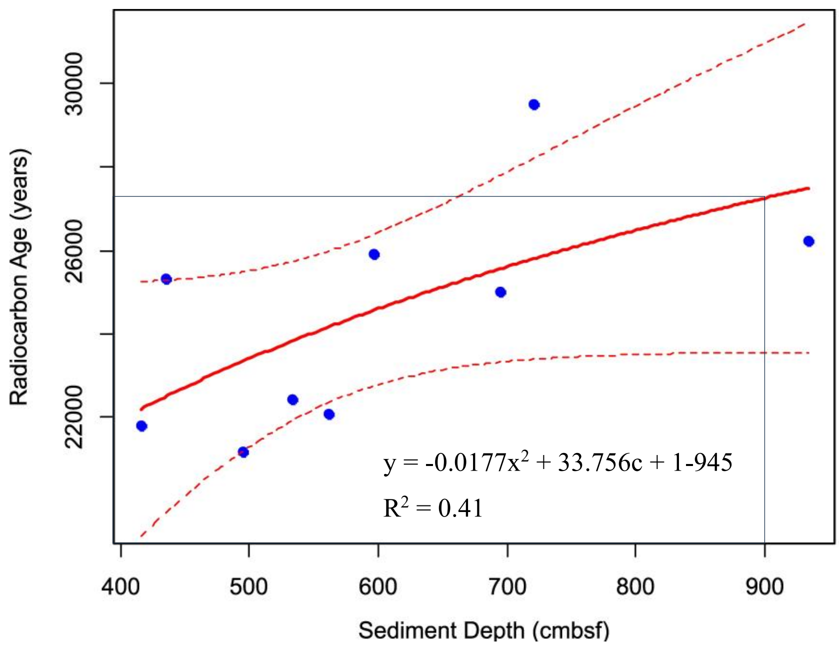

Figure S4: Radiocarbon ages from cores collected on the 2015 survey cruise (Jenning et al., 2022). The regression model provides an approximate ~27,000 ±4,000-year age for slope sediments that are 9 mbsf. Dotted red lines mark 95% confidence intervals.

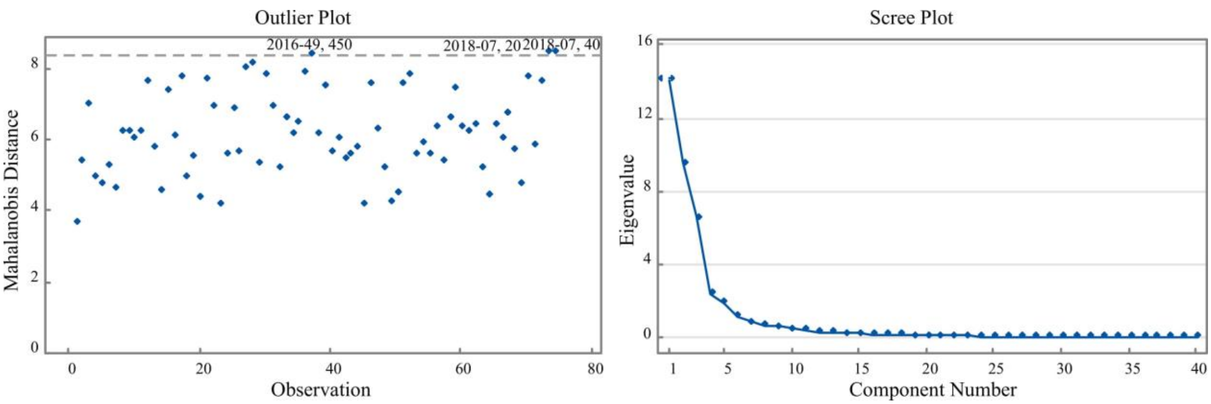

Figure S5: Mahalanobis distance outlier and scree plots for the principal component analysis of the 74 sediment samples.

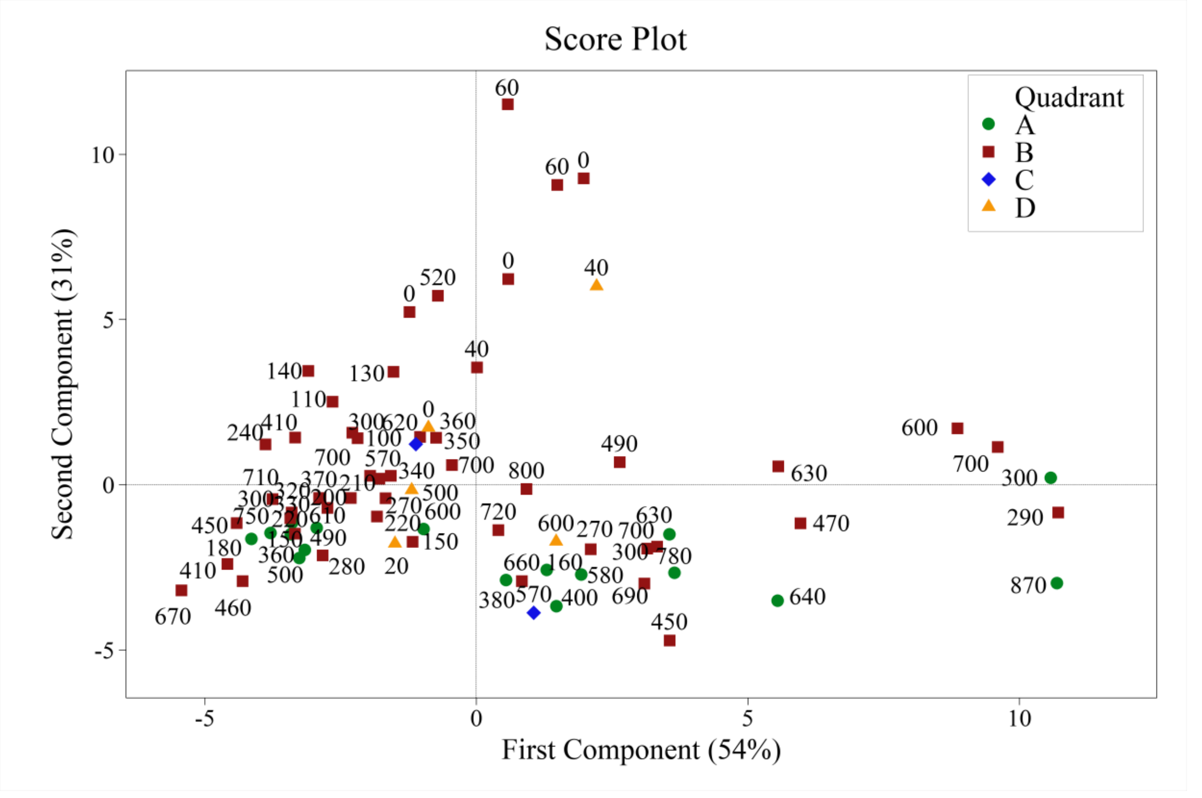

Figure S6: Principal component analysis of archaeal lipid concentrations in 74 sediment samples of Scotian Slope, highlighting the score plot in which sediment samples are grouped corresponding to the quadrants determined in Figure 1, with labels indicating the burial depth of each sample.

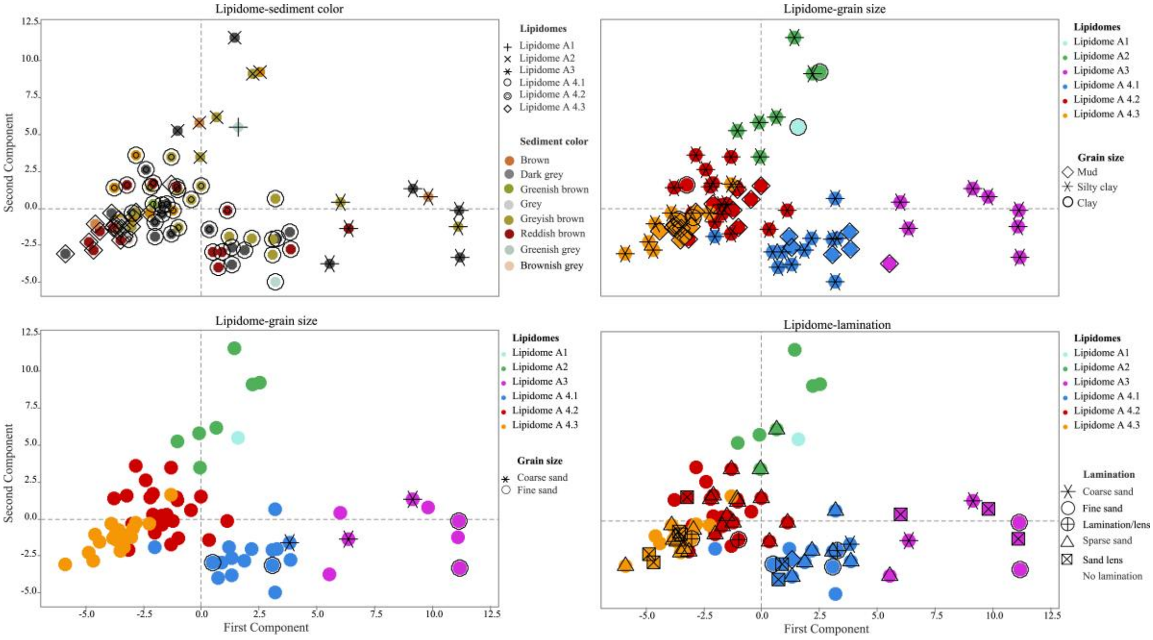

Figure S7: Principal component analysis plots each examining the relationship between lipidomes and lithological composition of the sediments: sediment color, sediment grain size, and lamination types.

S.2.1 References

Jenner, K. A., Campbell, D. C., Barnett, J. M., Higgins, J., and Normandeau, A.: Piston cores and supporting high-resolution seismic data, CCGS Hudson Expedition 2015018, Scotian Slope, offshore Nova Scotia, Canada, https://doi.org/10.4095/330088, 2022.